Water Resources Research

RESEARCH ARTICLE
10.1029/2019WR026988

Potential of a Gravity-Driven Film Flow Model to Predict Infiltration in a Catchment for Diverse Soil and Land Cover Combinations

D. Demand[1] and M. Weiler[1]

[1]University of Freiburg, Institute of Earth and Environmental Sciences, Hydrology, Freiburg, Germany

Key Points:

- Gravity-driven film flow has a large potential to describe preferential flow during natural infiltration events at a diversity of sites
- Parameters can be determined from the rainfall input, which has a stronger effect on the flow velocity than initial soil water content
- Abstraction of water from film flow in macropores into the soil matrix is a process that has to be included in more detail

Supporting Information:

Supporting Information may be found in the online version of this article.

Correspondence to:

D. Demand,
dominic.demand@hydrology.uni-freiburg.de

Citation:

Demand, D., & Weiler, M. (2021). Potential of a gravity-driven film flow model to predict infiltration in a catchment for diverse soil and land cover combinations. *Water Resources Research*, *57*, e2019WR026988. https://doi.org/10.1029/2019WR026988

Received 19 DEC 2019
Accepted 14 APR 2021

Abstract Applying physically based models that include preferential flow (PF) is still very challenging at the catchment scale. A gravity-driven film flow approach could be a promising concept for modeling PF as it only requires a small number of parameters. We tested if this approach can be used for different soils and land covers within a 247 km^2 catchment and if we can find generalizable relationships of the film flow parameters to site or rainfall properties. We used a unique data set from a soil moisture sensor network with 135 instrumented soil profiles in three different geologies (slate, marl, and sandstone) and two land covers (forest and grassland) and fitted the film flow model to around 1,700 infiltration events. The results demonstrate that the physical relationship of film flow was capable to predict wetting front velocity (v) and flow parameters from rainfall input (q_s) alone. This relationship was pronounced in grassland sites but weaker for forest sites, probably due to heterogeneity of the rainfall input underneath the canopy. Incorporating the water content into the v-q_s relationship did not improve the quality, but showed that for the film flow the rainfall input and hence gravity is in fact the dominant driver and not capillarity. Furthermore, abstraction of water into the soil matrix during film flow is an important process to be included into the framework with reasonable agreements for marl and sandstone using a multiple linear regression. Film flow and corresponding functional parameter relationships for other regions could improve catchment wide PF modeling in the future.

1. Introduction

Preferential flow (PF) in the unsaturated zone is a common phenomenon resulting in rapid water flow and solute transport during infiltration (Germann et al., 2007). PF often occurs in macropores with either abiotic (e.g., soil cracks) or biotic origin (e.g., soil fauna, root channels) (Beven & Germann, 1982). Soil hydrological models still suffer from difficulties in describing the heterogeneous and complex nature of PF, which often results in higher flow velocities than pure capillary-driven matrix flow (Germann & Hensel, 2006; Nimmo, 2007). Not including these fast flows when modeling infiltration can lead to problems predicting runoff formation (Beckers & Alila, 2004; Niehoff et al., 2002), solute transport (Gerke & Köhne, 2004; Haws et al., 2005) and stable water isotope dynamics (Sprenger et al., 2018).

In the past, many methods have been developed to overcome the challenge of describing PF in soils, such as models based on explicit network structures (Vogel & Roth, 1998) or approaches treating the initiation of macropore flow as infiltration or percolation excess and describing flow based on the macropore geometry (Armstrong et al., 2000; Weiler, 2005). Other approaches describing PF in soils are often based on continuum models adapting the Darcy-Richards theory (Richards, 1931). One of these methods includes the effect of macroporosity into the water retention relationship near saturation, to enable a single domain representation of PF (Durner, 1994; Iden & Durner, 2014). However, some studies demonstrated that PF does not only occurs in soils close to saturation (Nimmo, 2012; Weiler & Naef, 2003a). Therefore, dual-porosity or dual-permeability models are used separating flow into a fast PF domain and a matrix domain for storage or matrix flow, respectively (Köhne et al., 2009). In these dual-domain models the Richards equation was also frequently applied for the fast flow domain (Gerke & van Genuchten, 1993).

One alternative to the "classical" capillary-based physical models for infiltration (Darcy-Richards) is the gravity-dominated film flow model. Such a process was first observed experimentally by Tokunaga and Wan (1997). Or and Tuller (2000) derived such a film flow model by assuming laminar flow at rough surfaces. Jackisch and Zehe (2018) used a particle-based film flow scheme were the water film is decelerated by

friction and the exchange of water with the soil matrix. Kinematic wave approaches also fall into the group of gravity-based flow processes and exist as single domain models (Beven & Germann, 1981; Germann, 1985) or are used to describe flow in the macropore domain of dual-domain models (Jarvis et al., 1991; Larsbo et al., 2005). Germann and Di Pietro (1996, 1999) derived a film flow model based on Newton's hypothesis of shear flow that is only driven by gravity against the viscous momentum dissipation. A similar model has been presented by Nimmo (2010).

All the models introduced above face similar problems for application in hydrological models, as they require detailed information about the hydraulic properties, number, geometry, or structure of these pore-networks. These parameters vary with many landscape properties such as soil texture (Baer et al., 2009), land cover (Alaoui et al., 2011), land management (Shipitalo et al., 2000), and may further change over time (Reck et al., 2018). Hence, determining these model parameters is very challenging and a direct measurement can only be done for certain model types at small spatial scales (Kodesova et al., 2010; Logsdon, 2002; van Schaik et al., 2010). Therefore, the PF parameters are often calibrated (Arora et al., 2011; Köhne et al., 2002; Merz & Bárdossy, 1998). But the large number of parameters in these models to be calibrated make it difficult to find physically meaningful parameters for the macropore domain due to uncertainty and equifinality in calibration (Arora et al., 2012; Klaus & Zehe, 2010). When using Darcy-Richards capillary flow models for PF, the identification of physical meaningful and transferable parameters is even more challenging. The Richards equation imposes capillarity as a driver of flow, which is an incorrect representation of gravity-driven macropore flow (Jarvis, 2007). Other problems related to the Richards equation being used for modeling PF flow are non-equilibrium conditions (Diamantopoulos & Durner, 2012) and the small representative elementary volume under which it is valid (Vogel & Ippisch, 2008). Therefore, applying these kinds of models should be seen as a "conceptual approximation" rather than physically based (Beven & Germann, 2013).

As Beven and Germann (2013) propose, the popularity of an infiltration model reflects the availability of pedotransfer-functions to estimate the relevant model parameters, such as the retention-parameters for the Richards equation (e.g., Carsel & Parrish, 1988; Schaap et al., 2001). Functional relationships for estimating the properties of the macropore domain—similar to estimating the parameters of the soil matrix with pedotransfer-functions—rarely exist. The main reason may be the high spatial and temporal variability of these parameters, but also the lack of transferable parameter sets as described in the section above. An appropriate physical-based model of PF with predictable parameters for larger scale application at the catchment scale is still missing.

The gravity-based film flow model of Germann and Di Pietro (1999) has the potential to overcome these problems. The model only needs two basic parameters (neglecting potential interactions with the soil matrix) and has the advantage that it can be analytically solved. Furthermore, the film flow has less restrictive requirements than capillary continuum models concerning the representative elementary volume and can thereby be easier applied across scales (Germann & Karlen, 2016). Film flow can be kinematic in nature and integrates all flow into one flow domain (Germann, 2014; Germann & Karlen, 2016). The model has been intensively tested under a large numbers of laboratory and field plot experiments with defined boundary conditions (e.g., constant rainfall intensity with sprinkling experiments) (Germann & al Hagrey, 2008; Germann & Karlen, 2016; Germann & Prasuhn, 2018). Tests have been performed on the effect of the input flux, for example, rainfall (I. Hincapié & Germann, 2009a), the interaction of the macropore water film with the soil matrix, for example, water abstraction (Hincapié & Germann, 2009b) or the superimposition of multiple flow waves (Germann et al., 2007).

However, this film flow model framework has not been tested for its suitability to model infiltration for the diversity of situations than can occur at the catchment scale with a high variation of soil properties under different land cover and topographic positions and under natural rainfall characteristics. These variations include seasonal changes in the soil structure and numerous natural boundary conditions, such as a large variety of initial water contents, rain amounts and rain intensity distributions. Therefore, the potential of functional relationships for different landscape units (soils and land cover), similar to pedotransfer-functions was not examined for gravity-driven film flow. Hence, we will focus on the effect of input flux (rainfall) and storage state (initial soil moisture) on the soil water flux (flow velocity) and storage change (soil moisture change) using a gravity-driven film flow model.

Table 1
Overview of the Average Soil Properties for the Different Landscape Units

	Slate		Marl		Sandstone	
	Forest	Grassland	Forest	Grassland	Forest	Grassland
No. of soil moisture profiles	45	21	15	18	27	9
Main Texture (USDA classification)	silty clay loam	silty clay loam	loam/clay	clay loam/clay	sandy loam	sandy loam
Bulk density [g cm^{-3}]	0.93	0.86	1.14	1.21	1.21	1.53
Stone content (>2 mm Ø) [%]	33	31	2	7	0	1

In this study, we test the Germann and Di Pietro (1999) film flow model and optimize its parameters for a large data set of natural infiltration events derived from a soil moisture sensor network within diverse soil/vegetation combinations. We examine the optimized film flow parameters of soil water flux and storage based on the film flow physical properties and try to find simple functional relationships for each soil/land cover unit. Finally, we test the effects of rainfall intensity and initial soil water content on the flow velocity using a film flow model compared to a capillary flow model.

2. Material and Methods

2.1. Study Sites

For this study, a unique data set from an extensive soil moisture sensor network installed in the mesoscale Attert catchment (247 km^2) in the western part of the Grand Duchy of Luxembourg was used. The data set consists of 135 instrumented soil profiles, each with soil moisture sensors at three depths (10, 30, 50 cm). Sensors were installed horizontally from a 30 cm diameter hole with each sensor slightly shifted in the horizontal direction to the one above. Sensor cables were laid downwards in the hole first and led up on the opposite wall to prevent artificial PF along the cables. 5TE capacitance probes (METER Environment, USA) were installed, which measure the volumetric water content (θ) with an accuracy of ± 0.03 m^3 m^{-3} without calibration (DecagonDevices, 2016) and calculate water content by the permittivity—water content relationship of Topp et al. (1980). The temporal resolution of all measurements was 5 min. The data set used in this study covers the period from March 2012 (first profiles installed) or October 2013 (last installed profiles) until February 2017. During this time period, 43 probes were changed to SMT100 (TRUEBNER GmbH, Germany) and nine probes to GS3 sensors (METER Environment, USA) due to sensor failure. Three profiles were always in a close proximity to each other (max. 20 m) at 45 different sites. The 45 sites were distributed among three different geologies: Devonian Slate covered by periglacial slope deposits mixed with aeolian loess (slate), Jurassic Luxembourg Sandstone (sandstone), and Triassic Sandy Marls (marl). In the slate and sandstone region, profiles were mainly installed along hillslope transects, whereas in the flatter marl region the sites were more randomly placed. The soils that developed were Haplic Cambisols (Ruptic, Endosketelic, Siltic) on the slate, Colluvic Arenosols or Podzols on the sandstone, and Stagnosols on the marl due to clay layers in 20–50 cm depth (IUSS Working Group WRB, 2006). Furthermore, the sites were distributed among two different land covers: forest with European beech (*Fagus sylvatica*) as the dominant species, and grassland mainly used as pasture or sometimes as a meadow. Six landscape units were defined by the three main geologies, each with the two different land covers. The average soil characteristics of the six different landscape units can be found in Table 1. Texture and stone content was measured by sieving and sedimentation analysis following DIN ISO 11277 (2002) from random distributed samples of the upper 20 cm. Bulk density was determined from 250 ml soil cores also taken in the upper 20 cm that were dried and weighted. At each grassland site precipitation was measured with a tipping bucket (Davis Instruments, USA) with a resolution of 0.2 mm and a collection area of 214 cm^2. At each forest site, five tipping buckets were randomly installed and the mean was calculated to obtain a time series of average throughfall. If one tipping bucket did not record rainfall and at least three other tipping buckets recorded rainfall over a period of 2 h, this single non-recording tipping bucket was removed for calculating the mean.

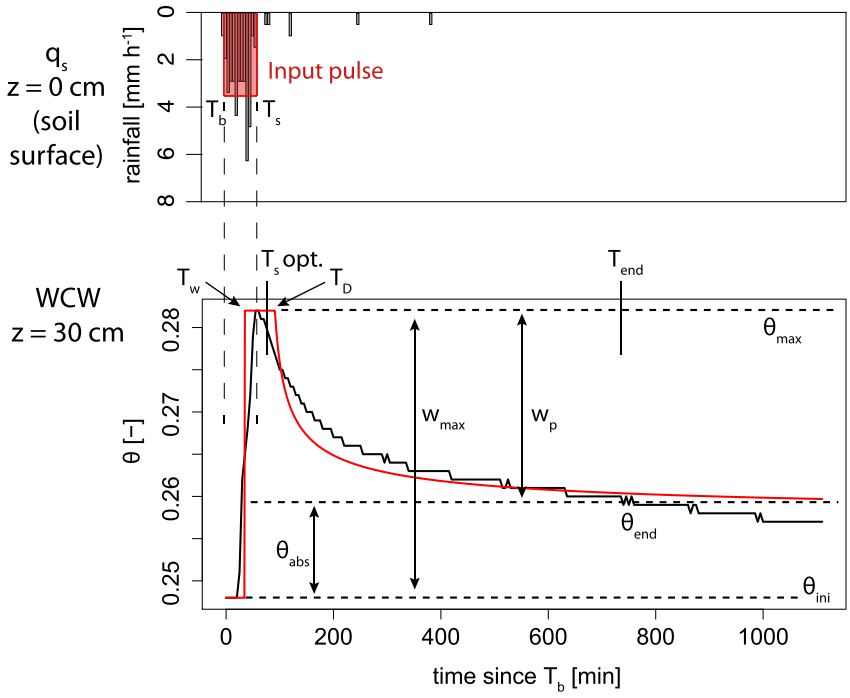

Figure 1. Schematic diagram of the rainfall pulse (upper part of the diagram) and the resulting WCW (lower part of the diagram) indicating all relevant parameters and variables. All parameters of the WCW besides T_b and T_s are a function of depth. T_{end} is not firmly specified. The black line shows measured water content (θ) whereas the red line shows the predicted WCW by the film flow approach. This diagram is based on a fitted curve of the M_A site, profile 1 on May 24, 2014 0:00. For an explanation of the parameter T_s opt. see the optimization Section 2.3. WCW, water content wave.

2.2. Principles of Gravity-Driven Film Flow

The film flow model represents a 1D steady-state viscous film flow with gravity being the only force against the viscous momentum dissipation, without any pressure or capillary forces being considered (Germann, 2014). The gravity-driven film flow approach was derived from Newton's shear flow hypothesis (Germann & Di Pietro, 1999) and is a special form of the kinematic wave (Jarvis et al., 2017), therefore also displaying kinematic properties (Di Pietro et al., 2003; Germann et al., 2007). Film flow is only valid under laminar flow conditions with Reynolds number of ≈1 (Germann & Karlen, 2016). The film flow concept can be adapted to various flow geometries (under steady-state assumptions) and thereby yields corresponding analytical solutions (e.g., Germann & al Hagrey, 2008; Germann et al., 2007). The influence of the assumed pore geometry on the flow was found to be relatively small compared to the other model assumptions (Germann, 2014). In this study, we use the solution for free-surface flow along a vertical plane. The following section briefly introduces the main concepts relevant to this study. The full derivation of the theory can be found for example in Germann (2014). The subsequent section follows the derivations of Germann and Karlen (2016) and Germann and Prasuhn (2018).

Defining a rectangular input pulse with a start time (T_b), end time (T_s) and a volume flux density q [L T^{-1}], that infiltrates into a porous medium like soil, a water film of maximum thickness F [L] is developed along pore walls that covers a vertical area per soil volume defined as the specific contact area L [L^2 L^{-3}]. The input pulse forms a water content wave (WCW) in the porous medium that is moving downwards with a mobile water content w_p [−] during flow defined by:

$$w_p = L * F = \theta_{max} - \theta_{end} \quad (1)$$

with θ_{max} and θ_{end} are the volumetric water content [−] at the peak and end of the WCW respectively (see also Figure 1 as illustration). This equation relates the flow in a certain pore network to its average water content properties.

Integrating the differential volume flux density of a water film from the solid-water to the water-air interface (for details see Germann, 2014 or Germann & Di Pietro, 1999), we obtain the volume flux density of the water film q [L T^{-1}]:

$$q\left(F,L\right)=\frac{g}{3\eta}\mathrm{LF}^3 \tag{2}$$

where η is the kinematic viscosity of water [L^2 T^{-1}] and g the acceleration due to gravity [L T^{-2}].

The wetting front arrives at a certain depth z at time T_w as a wetting front shock with a constant plateau of w_p (Figure 1). The mobile water content is $w(z, t) = 0$ for $t < T_w$ at depth z. The water film flows with a constant wetting front velocity v [L T^1] that is defined by:

$$v\left(F\right)=\frac{q\left(F,L\right)}{w\left(F,L\right)}=F^2\frac{g}{3\,\eta} \tag{3}$$

Equation 3 demonstrates that the wetting front velocity only depends on the film thickness F and on the gravity that forces flow against the resistance of viscous momentum dissipation. From the measured WCW the velocity can be calculated by the arrival time of the wetting front shock at a certain depth:

$$v=\frac{z}{\left(T_w\left(z\right)-T_b\right)} \tag{4}$$

With the end of the input pulse T_s, the maximum film thickness collapses to zero and a drainage front is released that is controlled by the speed of the fastest lamina. The resulting change in dq/dw is called the wave celerity c [M T^{-1}]:

$$c\left(F\right)=\frac{dq}{dw}=F^2\frac{g}{\eta}=3\,v\left(F\right) \tag{5}$$

When analyzing a WCW the celerity can be found by the arrival time of the drainage front that reaches the depth z at time T_D.

$$c=\frac{z}{\left(T_D\left(z\right)-T_s\right)} \tag{6}$$

Combining Equations 4–6 with $T_b = 0$ (starting time at 0 min), the relationship of T_w and T_D at depth z can be found by:

$$T_w\left(z\right)=3\,T_D\left(z\right)-3\,T_s \tag{7}$$

After T_D the mobile water content (w) at the depth z is decreasing with time (t). By reversing the integration of flow over all lamina, the depth-time distribution of the collapsing water film can be found (for details of derivation see Germann & Karlen, 2016).

$$\mathrm{w}\left(\mathrm{z},\mathrm{t}\right)=\mathrm{F}\,\mathrm{L}\left(\frac{T_D\left(\mathrm{z}\right)-T_s}{t-T_s}\right)^{1/2} \tag{8}$$

The WCW has not necessarily to decrease back to the initial water content θ_{ini} due to abstraction of water into the soil matrix. Therefore, we define the water abstraction of a WCW to the soil matrix θ_{abs} [−] as:

$$\theta_{\mathrm{abs}}=\theta_{\mathrm{end}}-\theta_{\mathrm{ini}}=w_{\mathrm{max}}-w_p \tag{9}$$

with θ_{end} being the final volumetric water content [−] and w_{max} [−] the mobile water content increases from θ_{ini} to the peak of the WCW (Figure 1).

Between $T_w(z) < t < T_D(z)$ the volume flux density at the soil surface q_s [L T^{-1}] (rain pulse intensity) is equivalent to q: $q(z, t) = q_s$. By combining Equations 1–3 and eliminating F, we can predict v based on the rainfall or input intensity q_s:

$$v(q_s) = q_s^{2/3}\left(\frac{g}{3\eta}\right)^{1/3} L^{-2/3} \tag{10}$$

2.3. Estimation of Film Flow Parameters from a WCW

Due to difficulties involved in the direct measurements of film thickness (F), specific contact area (L), and water abstraction by the soil matrix (θ_{abs}), it is widespread to determine such parameters from measured WCWs (e.g., Hincapié & Germann, 2009b). In this study, parameters of the film flow model were determined by fitting simulated WCWs to the measured soil moisture reactions of the 135 instrumented soil profiles. Therefore, for every defined infiltration event and instrumented soil profile, we checked for a water content reaction at the three depths and obtained θ_{ini}, θ_{max}, and θ_{end} from the measured WCW. Using the relationships introduced in Section 2.2, a WCW was then calculated and optimized for T_w or T_D to fit the measured data at each reacting soil depth. From this optimized WCW, the wetting front velocity (v) and the parameters F, L and θ_{abs} can be determined, being the integrated parameters from the point of the pulse application (soil surface) to the depth of the sensor (Figure A1).

For defining infiltration events we used the 5-min resolution rainfall data of our sites. An event is defined when a minimum of 1 mm of rain falls followed by at least three consecutive hours without rain. If a soil moisture increase of at least 1 vol.% was detected during 48 h after the rainfall event ended or until the next event started, it was considered to be an infiltration event. If a new rain event was detected within 6 h after one event, both events, the previous and the following, were not considered in the analysis to have clear separated WCWs. Infiltration events were tested for plausibility considering rainfall amount and intensity, and only events that showed a sensor response in sequence from top to bottom were further analyzed.

The analytical solution of the film flow concept requires a single rectangular input pulse (Germann & Karlen, 2016), despite the fact that rainfall events are rarely uniform. Hence the observed rainfall events had to be transformed into a rectangular pulse. A linear regression was fitted to the cumulative rainfall amount of each infiltration event using the data between the 0.25% and 0.75% quartile of the density distribution of cumulative rainfall (Figure 2). Thus, a rain pulse can be defined with uniform rainfall characteristics during the phase of the major event rainfall. The duration of the rain pulse can then be found by taking the x-axis intercept of the regression equation as the beginning and the intercept of the regression with the total rainfall amount as the end point. The slope of the regression defines the mean pulse intensity (q_s). We considered only rain pulses with ≤3 h for the analysis as the intensities of longer events tend to be more fluctuating and a clear rain pulse can hardly be defined. Furthermore, events with a mean air temperature lower than 0°C were not considered to exclude snowfall or frozen soil conditions. The empirical cumulative density distribution of rainfall pulse intensities of the resulting infiltration events can be seen in Figure 2b.

The WCWs were further checked for plausibility in the θ data and events that were caused by an oscillating signal (increase in soil moisture, but not more than three different θ values during the event; using $T_{end} = T_s + 12$ h) were removed. We also excluded events with water contents at or near saturation ($\theta > 0.65$). WCW modeling was done at a one-minute resolution. Therefore, the 5-min measured soil moisture data was used for the five following minutes in a one-minute resolution. The potential error in determining the wetting front velocity, which may be caused by the temporal resolution of the soil moisture measurements, is described and estimated in the Supporting Information (Text S1, Figure S1). Since the kinematic viscosity (η) is a function of temperature it was calculated according to Weast (1989) from soil temperature in the respective depth under the assumption that rainwater temperature in the thin water films equilibrates quickly to the soil temperature.

Using these input pulses and related infiltration events, a global optimization (GLO) of T_w and T_D was found to be the best method to project the measured WCW. A comparison of different optimization methods can be found in the Supporting Information (Text S2, Figure S2 and Table S1–S3). The fit accounts for the arrival time of both, the wetting front and the draining front with the relationship of $c = 3v$ (Equation 5).

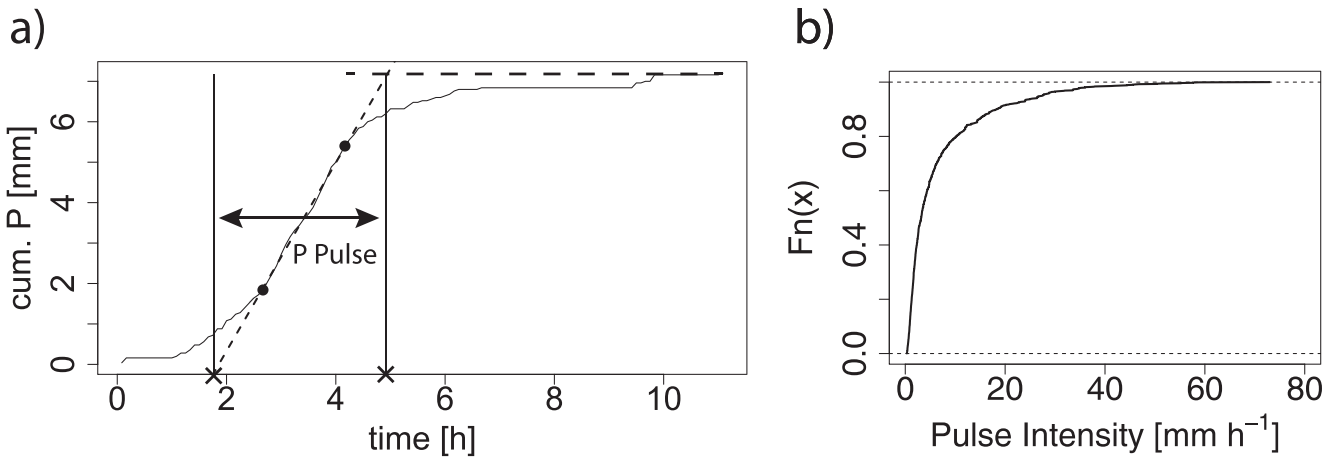

Figure 2. (a) Example of cumulative rainfall (cum. P) with time used for the transformation of a rainfall event to a rain pulse and (b) the resulting empirical cumulative density function of intensities for every infiltration event with rainfall duration ≤3 h.

Additionally, the method optimizes for T_b and T_s, as the beginning and end of the rainfall pulse strongly influences v and c (see Equations 4 and 6). Hence, the GLO method accounts for the uncertainties introduced by defining the rectangular rain pulse. The range of T_b was limited as an upper boundary by the time when a change in water content ($\Delta\theta$) during the WCW of 0.002 was reached, unless θ increased by more than 0.002 in the first 10 min (then T_b was not optimized and taken from the rainfall pulse). Furthermore, the uncertainty of T_s was limited to an upper maximum of $T_s + 2$ h. Since it is difficult to firmly define the end of the WCW, T_{end} was also included into the fitting approach. Using T_{end} in the optimization further allows to exclude possible influences of new rain events, which could occur at the end of the WCW. $T_s + 8$ h was chosen as a lower limit for T_{end} to ensure that the draining front is also included in the fit. The upper limit for T_D was defined by constraining $T_w < T_D$, and hence by the upper limit of T_s and Equation 7. Upper and lower limits of the initial parameter ranges can be found in Table 2.

For the global optimization we used the Differential Evolution Algorithm (Storn & Price, 1997) implemented in the *R* package DEoptim (Mullen et al., 2011). Each population had 200 iterations/population generations and the modified Kling-Gupta efficiency (KGE) (Kling et al., 2012) was used as objective function (calculated for the $\Delta\theta$ of the WCW starting at T_b).

We used a set of rules to avoid WCWs with irregular shapes being fitted to the observed soil moisture data. Modeled WCW fits that do not show a θ decrease from θ_{max} of more than 0.002 until T_{end} (e.g., due to a T_{end} that is too short) and events with an optimized T_D that miss the center of the θ_{max} peak by more than 60 min were set to KGE = −2 to avoid such a fit. However, since some measured WCWs showed no θ decrease of 0.002 from θ_{max} until the last possible T_{end} (the mean θ of the last 10% of the observations was used), these soil moisture observations did not reveal a clear WCW shape (very low w_p) and hence fitted parameters were excluded from further analysis. Potential reasons for such behavior could be the complete adsorption (θ_{abs}) of the infiltrating water into the soil matrix, waterlogging or inaccuracy of the soil moisture sensor. In addition, WCW fits with KGE < 0.5 and a fitted T_w that misses the beginning of the θ_{max} peak by more than 3 h do not reflect θ behavior similar to the film flow characteristics and can be caused by one of the aforementioned reasons or a flow process that is different from film flow. An oscillating soil moisture signal (not more than three different θ values) that emerged due to a shortening of the WCW when optimizing for T_{end} were removed from the analysis as well.

One problem with the optimization was found with fits that tended toward $T_D \approx T_s$, whereby the velocity trends toward infinity. A maximum velocity of 0.014 m s^{-1} was used to filter out these events, which corresponds to a film thickness of around 65 μm at 20°C. This film thickness can be seen as a restriction of laminar flow (Re < 1) and was thereby assumed to be an appropriate criterion, since higher flow velocities violate the assumptions of film flow (Germann & Karlen, 2016).

Table 2
Overview of the Initial Parameter Ranges of the Optimization Procedure

	T_b	T_s	T_{end}	T_D
Lower limit	0 min	1 min	T_s + 8h	1 min
Upper limit	$\Delta\theta < 0.002$	T_s + 2h	T_s + 12h	T_s + 7.5 h

2.4. Analysis of the Obtained Film Flow Parameters

The optimized film flow parameters of the measured WCWs were first analyzed for their general properties and differences between the lithologies and land covers. Subsequently, the fitted values were used to derive and evaluate the following relationships.

2.4.1. Testing a Functional Relationship of Wetting Front Velocity and Rainfall Pulse Intensity

For applying the film flow model for soil water flux, only two basic parameters must be determined: F and L.

Defining a velocity-modulation coefficient (a) for Equation 10 yields a power law relationship between v and q_s with the exponent 2/3:

$$a = \left(\frac{g}{3\eta}\right)^{1/3} L^{-2/3} \tag{11}$$

$$v\left(q_s\right) = a\, q_s^{\,b} \quad b = 2/3 \tag{12}$$

F and L can be predicted from the input flux pulse (rainfall intensity) alone when knowing the parameter a from the v-q_s relationship (Equation 12). However, this relationship only holds if infiltration in natural soils follows the rules of film flow and thus the exponent b in Equation 12 is 2/3. The validity of this assumption was indicated in a laboratory experiment of Hincapié and Germann (2009a) for an undisturbed soil column, but it certainly needs further validation under natural soil and rainfall conditions. If we assume steady-state and furthermore no change of L with the rainfall intensity ($dL/dq_s = 0$), a slope of 2/3 (exponent b in the power law) in a log-log diagram plotting q_s against v should be found. This would allow prediction of L with Equation 11 and F with Equations 12 and 3. Hence, the film flow theory has the potential to directly provide a straight functional relationship with only one free parameter (a) that needs to be related to some landscape properties, such as for example, soil type or land cover. We analyzed the parameters (a, b) of the power law v-q_s relationships (Equation 12) for all infiltration events observed in the different landscape units (all instrumented soil profiles; instrumented soil profiles of a certain geology or geology/land cover combinations) with respect to the assumptions of film flow.

2.4.2. Evaluating the v-q_s Relationships to Predict Soil Water Flow

We evaluated the predicted parameter sets (a, b) for plausible functional film flow relationships. We used these relationships to predict F or $F + L$ for each infiltration event and compared the predicted results against the soil moisture measurements (θ) or against the optimized wetting front velocities (v).

We evaluated two cases: (i) The prediction of the wetting front velocity and parameter F based on the optimized relationships of v-q_s. In this case L was taken from the optimized values of the individual events and F was calculated from v (Equation 3). (ii) The prediction of the parameters F and L together, assuming an exponent $b = 2/3$ in the v-q_s power law relationship. We used the median kinematic viscosity for each landscape unit and for the observed depths (10 or 30/50 cm) to calculate F and L from the v-q_s relationship.

Since F and L also influence the mobile water content (Equation 1), their prediction can also influence θ_{end}. The water abstraction by the soil matrix (θ_{abs}) were taken from the optimization, thus the performed evaluation only provides information on the error of the water content change prediction related to the parameters F and L. The predicted change in water content ($\Delta\theta_{pred}$) from θ_{ini} to θ_{end} was compared against the change of the measured WCW for the same time period ($\Delta\theta_{obs}$). Hence, the error between the predicted and the measured θ_{end} can be estimated (error $\theta_{end} = \Delta\theta_{obs} - \Delta\theta_{pred}$).

2.4.3. Termination Criterion for the Film Flow Process

A termination criterion for the film flow process is necessary since the mobile water content (w) asymptotically converges to the water content at T_{end} (θ_{end}). The termination criterion influences the predicted water content change ($\Delta\theta_{pred}$) and is needed to compare the error in $\Delta\theta$ (see section before). This criterion can also be interpreted as a switch to a different flow process (e.g., capillary flow).

For our parameter calibration we included T_{end} as part of the optimization to achieve an optimal WCW, but this point in time is without a clear physical meaning. For application of film flow infiltration (no optimization) we decided to defined a criterion based on the decline of the optimized $w(z,t)$ with time to find T_{end}. Therefore, we introduced a parameter S as a value between 0.05 and 0.4 (0.01 steps) which describes the decline of $w(z,t)$ as a portion of $w(F,L)$.

For each value of S and all WCWs the point in time was determined where (Figure 3):

$$S * w\left(F,L\right) = w\left(z,t\right) \tag{13}$$

For all of these points in time the error (E) in soil water content (difference between the predicted and observed θ) was calculated and the errors of each S value were added up:

$$E_{sum} = \sum_{j=1}^{N} \left| E_j \right| \quad N: \text{number of infiltration events} \tag{14}$$

The S value with the lowest sum of errors (E_{sum}) was chosen as the best overall decline parameter (S_{opt}) to estimate T_{end} in model application using the approach described above (Equation 13).

2.4.4. Introducing the Effect of Soil Water Content on Gravity-Driven Film Flow and Comparison with Capillary Flow

The gravity-driven film flow model presented in Section 2.2 does not depend on the state of the soil water storage (soil water content) as other infiltration models do (e.g., Richards equation). To test this model assumption with our data, we included the initial soil water content (θ_{ini}) of each simulated infiltration event to the power law of the film flow model (Equation 12):

$$v\left(q_s,\theta_{ini}\right) = a\, q_s^b\, \theta_{ini}^n \tag{15}$$

with n being a power law parameter. This equation represents a multiple linear regression in the log-log space. It is important to note that this relationship is not based on the physical basis of gravity-driven film flow as presented in Section 2.2. However, a power law was also used by for example, Campbell (1974) to describe the relationship of water content and hydraulic conductivity.

We fitted these relationships to the values obtained by the WCW and received a functional relationship including both, the pulse intensity q_s and the initial soil water content θ_{ini}. To analyze the importance of q_s and θ_{ini} in the film flow model and evaluate the basic properties of the derived functional relationship we compared it with a capillary based model implemented in HYDRUS 1D (Šimůnek et al., 2013). To provide comparable conditions, the soil properties of HYDRUS 1D were parameterized based on functional relationship with soil types (pedotransfer-function).

We simulated capillary driven flow using HYDRUS 1D for three hypothetical soils with textures similar to our three geologies. We used the retention function of van Genuchten (1980) with an air-entry value of 2 cm (Ippisch et al., 2006) and the parameters of Carsel and Parrish (1988) for a silty clay loam (slate), clay loam (marl) and sandy loam (sandstone). An atmospheric boundary was set as upper boundary and free drainage was assumed for the lower boundary condition (domain height 4 m). Furthermore, surface runoff was considered when rainfall rate exceeds infiltration rate to avoid water ponding and hence a pressure buildup at the soil surface. Opposite to film flow, flow velocity calculated by Richards equation depends on the pulse duration (and thereby on the amount of rain). Therefore, the upper boundary flux was set constant to calculate the highest possible velocity under the assumed rainfall intensity. We ran the calculation for all

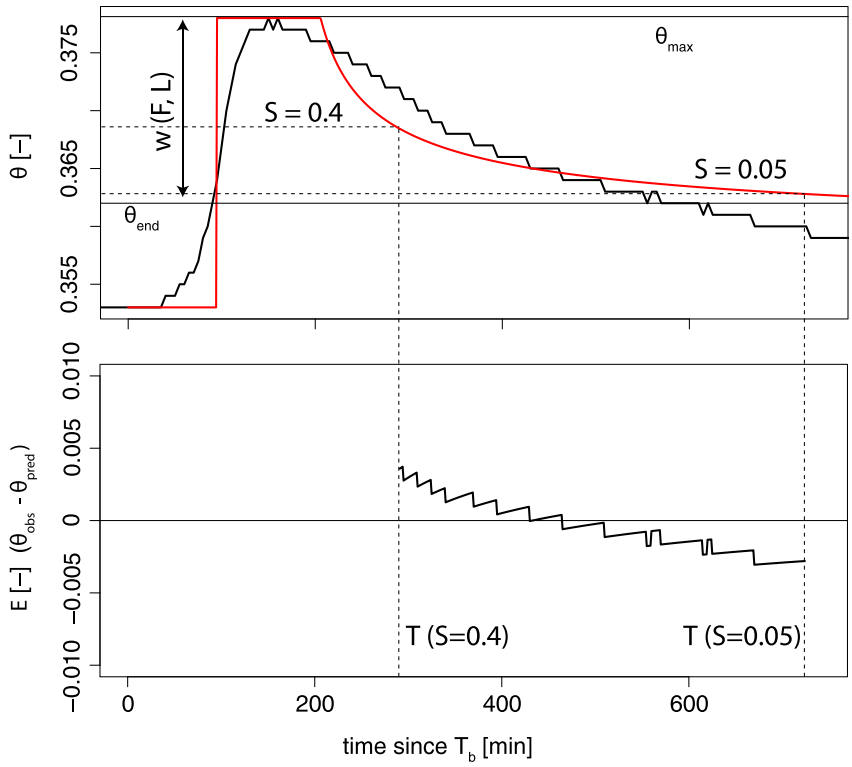

Figure 3. Schematic diagram showing the definition of the termination criterion based on the parameter *S* (upper plot) and the resulting error in soil water content (lower plot) representative for one WCW. In the upper plot the black line illustrates the observed data (θ_{obs}) whereas the red line shows the optimized WCW (θ_{pred}). WCW, water content wave.

combinations of q_s (rainfall intensity) from 2 to 30 mm h^{-1} (2 mm h^{-1} steps) and initial soil water contents from 0.2 to 0.4 (0.02 steps).

Wetting front velocities of the wetting fronts simulated with HYDRUS to 30 cm depth were calculated based on a regression method that was also tested as one of the optimization methods (REG) and can be found in the Supporting Information (Text S2). These results were compared against the wetting front velocity predicted by the fitted film flow parameters (Equation 15) in the grassland sites of all lithologies, with the same intensities and soil moisture contents. Since the film flow parameters are optimized for our data, whereas the capillary flow parameters (HYDRUS 1D) are not, we only compared relative increase in wetting front velocity (v_{rel}) to analyze the general model tendencies. This relative increase in wetting front velocity is calculated as:

$$v_{\mathrm{rel}} = \frac{v\left(q_s, \theta_{ini}\right)}{v\left(q_s = 2\ \mathrm{mmh^{-1}}, \theta_{\mathrm{ini}} = 0.2\right)} \tag{16}$$

2.4.5. Soil Water Storage in the Gravity-Driven Film Flow Model

As shown in Figure 1 or by Hincapié and Germann (2009b) the soil water content at the beginning (θ_{ini}) and end (θ_{end}) of the WCW are not identical, due to water abstraction or retention in the soil matrix (θ_{abs}). This storage property of soils is not directly included in the film flow approach yet, but should be considered when using the film flow model not only to predict water fluxes (e.g., wetting front velocity) but also quantifying the soil water storage change or retention.

Germann and Beven (1985) added a sink term [T^{-1}] to account for water abstraction dependent on the wave celerity, macropore water content, and water sorbance into the soil matrix. Hincapié and Germann (2009a) used a multiple linear regression model to predict the final water content including the input

flux and initial soil water content as predictors. We tested a similar approach with a multiple linear regression model to predict θ_{abs} for each event, accounting for the initial water content (θ_{ini}) as factor of matrix capillarity, the rainfall amount (P_{sum}) as the potential available water volume for abstraction, the optimized specific contact area (L) as a factor of potential abstraction area, z of the sensor depth and T_D–T_w as a proxy for the contact time:

$$\theta_{abs} = \alpha_1 \theta_{ini} + \alpha_2 P_{sum} + \alpha_3 L + \alpha_4 z + \alpha_5 \left(T_D - T_w\right) + \beta \quad (17)$$

with α_1 to α_5 and β being the regression coefficients. The linear model was fitted individual to all θ_{abs} values of each of the six landscape units (three geologies each with two different land covers).

3. Results

3.1. Film Flow Parameters of the Fitted WCWs

We analyzed in total 1,184 rainfall events at the different sites (one site had three instrumented soil profiles) that led to 1,718 infiltration events (on the level of a profile) of which 1,704 met the quality criteria (without oscillating signal or saturation) at 10 cm depth, 395 of those infiltration events also produced an usable soil moisture reaction in 30 cm and 136 in 50 cm. Hence, in total 2,235 WCWs could be used for optimizing the film flow parameters. Ten of the 135 instrumented soil profiles did not show a single infiltration event (≤3h), which was partly due to data gaps in the soil moisture time series. Around 62% of the measured soil moisture responses could be described with the film flow approach (for details see Supporting Information Table S2). Most WCWs were excluded since the measured peak water content (θ_{max}) was not decreasing by more than 0.002 (721 WCWs). Furthermore, only three WCWs with potentially non-laminar flow conditions were excluded and 115 due to an inappropriate fit (KGE < 0.5; T_w misprediction; too short T_{end} leads to inappropriate WCW). The soil moisture responses which could not be fitted show a significant lower soil moisture and rainfall pulse intensity ($p < 0.05$, Mann-Whitney, two-sided).

To investigate the film flow characteristics we compared the results with respect to the six main landscape units: three different geologies with two different land covers. The proportion of events that could be fitted varied between 53% for sandstone grassland and 69% for slate forest. Median KGE was similar among the landscape units ranging from 0.88 to 0.91. The empirical cumulative distributions of the parameters are displayed in Figure 4. Most wetting front velocities obtained by the optimization were between 10^{-5} and 10^{-3} m s^{-1} and the corresponding F values range between 2×10^{-6} and 18×10^{-6} m (2–18 μm). Sandstone showed more events with low wetting front velocities and low mobile water contents (w_p) than the other landscape units did. L was found to be strongly variable among events of the same plot. No large differences among landscape units can be seen for the L parameters beside of slate grassland showing higher L values than the other units do. This was related to the higher w_p values of the slate grassland than the other landscape units but similar flow velocities. The parameter θ_{abs} did not reveal systematic differences with geology or land cover and ranges mainly between 0 and 0.1. Only θ_{abs} showed a distribution similar to a normal distribution.

Statistical differences in wetting front velocity between the depths, land covers and geologies were tested using a Dunn test (Bonferroni correction). The wetting front velocity significantly increased with depth ($p < 0.01$). Additionally, if strictly comparing velocities between different response depth of the same events approximately 92% of wetting front velocities reaching a depth of 30 or 50 cm had a higher velocity than in 10 cm. Since the number of 50 cm reactions is rather low and the strongest increase in wetting front velocity can be seen between 10 and 30 cm, we analyze the set of 0–30 cm and 0–50 cm optimized wetting front velocities collectively (Table 3; see Figure A1 in the appendix for a schematic representation).

Forest showed significant higher wetting front velocities than grassland ($p < 0.01$). Furthermore, slate and marl exhibited a significant ($p < 0.01$) difference to sandstone, with marl having the highest wetting front velocities followed by slate and sandstone. For the same geology, forest profiles showed higher median wetting front velocities and standard deviations than grassland, except for marl in 10 cm (Table 3). The trend of sandstone sites with lower flow velocities than the clay-rich slate and marl was more evident in the grasslands. Highest variability in wetting front velocity was observed in the subsoil (30/50 cm depth) of the forest sites.

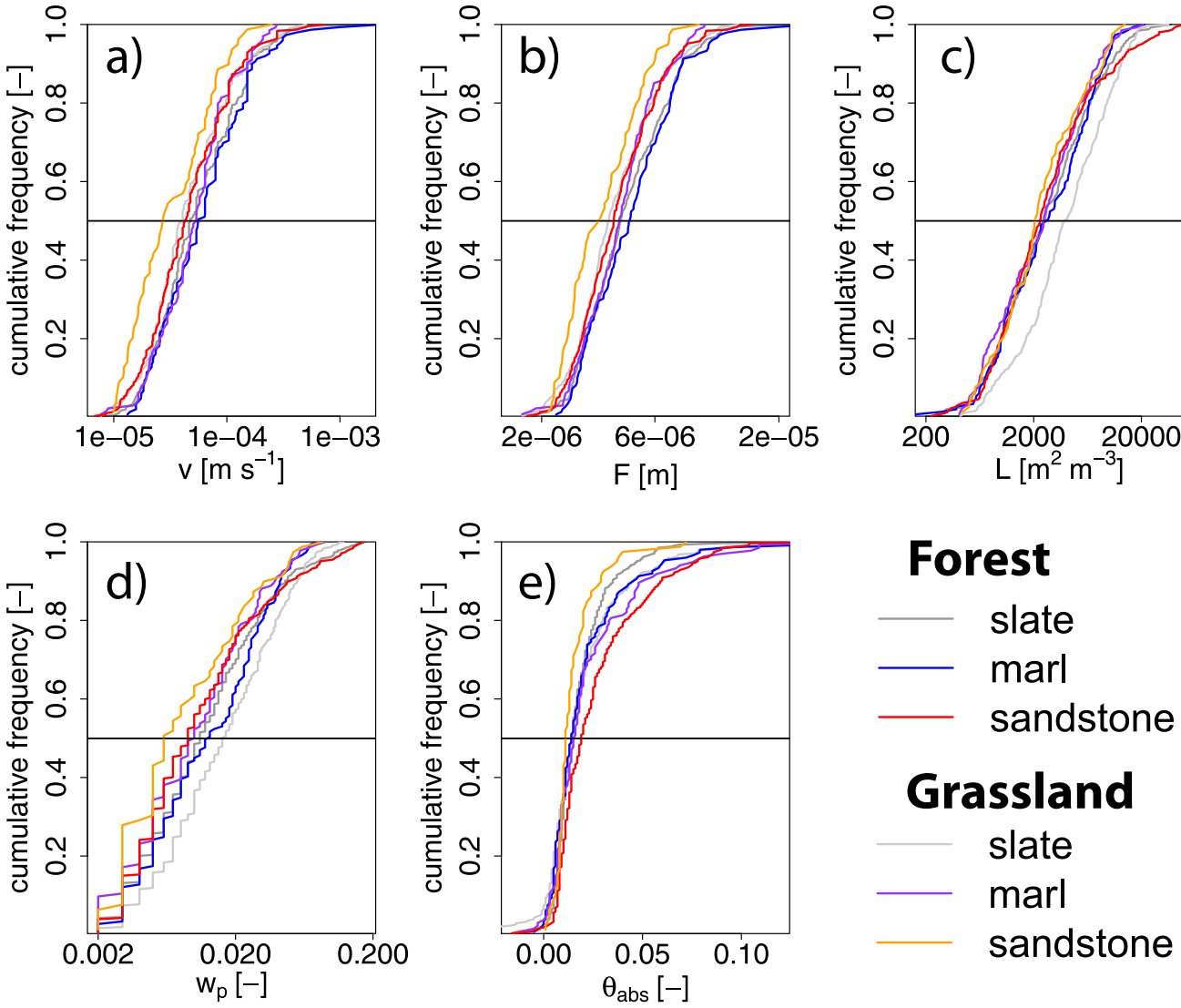

Figure 4. Empirical cumulative distribution of the parameters extracted from the WCWs (optimization) showing (a) the wetting front velocity v, (b) film thickness F, (c) specific contact area L, (d) peak mobile water content w_p and (e) water abstraction by the soil matrix θ_{abs}. WCW, water content wave.

3.2. Functional Relationship of Wetting Front Velocity and Rainfall Pulse Intensity

According to the theory of film flow the wetting front velocity should depend on the rainfall pulse intensity (q_s). These relationships were investigated separately for the six landscape units and two depth classes to test if this physical relationship holds in a high diversity of soil types and boundary conditions. Equation 12 describes the relationship between v and q_s with an exponent of 2/3 and a velocity-modulation coefficient a (Equation 11). Assuming a similar velocity-modulation coefficient a for all profiles within one landscape

Table 3
Median Optimized Wetting Front Velocities (v) [10^{-5} m s^{-1}] and Standard Deviation (Brackets) for the Six Landscape Units With Depth Obtained From the Optimization

	Forest			Grassland		
Depth [cm]	Slate	Marl	Sandstone	Slate	Marl	Sandstone
10	3.71 (4.68)	4.63 (5.64)	3.70 (5.16)	3.33 (5.38)	4.98 (4.92)	2.25 (3.27)
30/50	12.20 (19.42)	12.20 (42.27)	10.00 (14.83)	9.80 (10.54)	8.63 (7.57)	4.31 (5.90)

unit, a slope of 2/3 for a linear regression should be observe for log transformed variables v and q_s. Due to the relationship of v with both, q_s (Equation 12) and F (Equation 3), also a relationship of q_s with the parameter F can be derived (see Appendix Equation A1). This relationship is shown for the six landscape units and the two depths in the Appendix Figure A2 to visualize the transfer-function. Constraining the exponent b to the theoretical value of 2/3 (Equations 11 and 12), the velocity-modulation coefficient a can further be approximated for each landscape unit and used to predict an average L (see Appendix Table A1).

Table 4 illustrates the parameters of the q_s–v relationships for the two defined depths and six landscape units. The exponent b for all landscape units and depths ranged between 0.33 and 0.58. The exponent was lowest for the 30/50 cm depth of the forest sites. Furthermore, more variance is explained in the grassland plots than in the forest. The sites of landscape units with a higher explained variance could be seen as more homogenous in terms of film flow infiltration. In general, we observed for the different subgroups of the instrumented soil profiles (all data, different geologies or landscape units) that the exponent b of the v-q_s relationship showed a tendency to increase toward the expected 2/3 with increasing explained variance of the fit (Figure 5).

3.3. Evaluation of the v-q_s Relationships to Predict Soil Water Flow

The derived v-q_s relationships at the level of the different landscape units were tested for resulting errors when be used to model every infiltration event. The evaluation was performed for the grassland sites only since the explained variance of the v-q_s fits for the forests was rather low and the b values showed a higher deviation from the expected value of 2/3. We evaluated the functions for both, the resulting error in wetting front velocity (predicting v or F from q_s) and the discrepancy in the water content change ($\Delta\theta$) since F also influences w_p (Equation 1). If the theoretical value of b equal 2/3 holds, only the coefficient a for a specific site has to be determined to predict v and $\Delta\theta$ (ignoring θ_{abs}) for a given rainfall pulse. Therefore, we tested the error assuming $b = 2/3$ (not using the fitted b value) and again calculated v and $\Delta\theta$. Here we also used the average L value (Table A1) that can be derived under b equals 2/3. We compared the predicted wetting front velocity (v_{pred}) and water content change ($\Delta\theta_{pred}$) to the optimized velocity of the WCW (v_{obs}) and observed water content change ($\Delta\theta_{obs}$).

Table 5 shows the median, quartiles and maximum of the θ_{end} error, the goodness of the fit (KGE) and the best termination criterion (S_{opt}) for the two evaluation cases. A maximum of 21 WCWs (~4% of fits) could not be predicted using the $F + L$ prediction (exponent = 2/3), because the predicted velocities result in $T_w > T_D$. Furthermore, 10 modeled WCWs had to be excluded using the $F + L$ prediction, as the end criterion of film flow lead to a WCW that coincided with a second following event.

The predicted parameters F or $F + L$ reduced the KGE compared to the optimization, indicating that the shape of the WCWs is not well represented anymore. However, v_{pred} was still in good agreement to v_{obs} (Figure 6). By just predicting the wetting front velocity using the fitted relationship of v to q_s, modeled velocities were underestimated for the range of higher observed values ($v_{obs} > 2 \times 10^{-4}$ m s $^{-1}$). The prediction of $F + L$ (exponent = 2/3) was not changing the explained variance of the calculated wetting front velocity of all grassland sites, but the error becomes more normal distributed. Furthermore, the range of error in θ_{end} was getting larger using $F + L$ (Table 5), but as Figure 6 indicates, θ_{end} was still in high agreement with the observed values.

3.4. The Effect of Soil Water Content on Gravity-Driven Film Flow and Differences from Capillary Flow

The original gravity-driven film flow model did not include an influence of water content. We expanded the film flow model by the influence of initial water content to test for its influence. The resulting parameters of the expanded power law function to predict the wetting front velocity (Equation 15) are depicted in Table 6. Introducing the initial water content (θ_{ini}) as a predictor is only adding little explained variance (compare to Table 4). Furthermore, the effect of θ_{ini} on v is quite small and variable. The wetting front velocity can either increase or decrease with decreasing θ_{ini}, dependent on the landscape unit and depth. Especially in the topsoil (10 cm) the wetting front velocity often decreases with increasing θ_{ini}. The exponent b was relatively constant and only slightly changed compared to Table 4 when introducing θ_{ini}.

Table 4
Parameters of the q_s-v Trends From a Log-Log Relationship Following Equation 12

		10 cm			30/50 cm		
		a	b	R^2	a	b	R^2
Forest	Slate	0.0041	0.34	0.23	0.0100	0.33	0.24
	Marl	0.0167	0.41	0.31	0.0162[a]	0.34[a]	0.12
	Sandstone	0.0204	0.45	0.42	0.0102	0.35	0.20
Grassland	Slate	0.0175	0.46	0.44	0.1026	0.54	0.43
	Marl	0.0077	0.38	0.43	0.0288	0.44	0.52
	Sandstone	0.0485	0.55	0.73	0.1131	0.58	0.84

[a]Indicates non-significant ($p > 0.05$) parameters.
Note. a is the velocity-modulation coefficient and the exponent b the slope of the linear log-log trend.

We only used the models with the better fits of the more homogenous grassland sites in 30/50 cm to compare their reaction with the capillary flow model HYDRUS 1D. The non-optimized pedotransfer-function of HYDRUS 1D resulted in a magnitude smaller wetting front velocities (1.7×10^{-6}–5.7×10^{-5} m s^{-1}) compared to our optimized film flow model (2.1×10^{-5} m s^{-1}–2.4×10^{-4} m s^{-1}). For more details on the absolute values see Supporting Information (Table S4).

To visualize the general influences of q_s and θ_{ini} on wetting front velocity for the two methods we defined the relative increase in wetting front velocity (v_{rel}). Figure 7 shows the increase in v_{rel} with θ_{ini} and q_s for both models and for all three lithologies. Missing values in the HYDRUS 1D runs result from water content change that did not correspond to a wetting front of a WCW. In this case the results showed either a decrease of the water content (drainage of the profile; often observed for sandy loam with low q_s) or equilibrium flow with only little increase in water content ($\Delta\theta < 0.01$; often observed at high θ_{ini}).

Figure 7 shows v_{rel} being more similar for film flow (v_{rel} ~1–7) than for capillary flow (v_{rel} ~1–25) among the different soil types. The increase in wetting front velocity exhibited a stronger influence of soil type on capillary flow than on film flow. Second, we observed a very different shape of the relative wetting front velocity increase between the two models and driving variables. Film flow was strongly influenced by q_s, whereas capillary flow is more influenced by θ_{ini}. Even for the marl soils with the strongest influence of θ_{ini} on the film flow (parameter n in Table 6) a clear increase in v_{rel} was observed over the typical range of q_s values found in our study.

3.5. A Function for Soil Water Storage Change in the Gravity-Driven Film Flow Model

To assess storage change of the soil matrix (θ_{abs}) during film flow we tested a multiple linear regression model for each of the landscape units, based on five event properties (θ_{ini}, P_{sum}, L, z, T_D–T_w). The regression coefficients and the explained variance are depicted in Table 7. The models could explain between 13% and 49% of the variance. For each land cover, the highest R^2 was found for sandstone, followed by marl and slate. In all geologies, the forest sites showed a higher explained variance than the grassland sites. θ_{ini} and P_{sum} revealed a consistent influence (often significant) for all landscape units. θ_{abs} decreased with higher θ_{ini} and a higher P_{sum} led to an increase of θ_{abs}. The trend for L (positive trend) and z (negative trend) was, beside of one landscape unit each, also consistent. The positive trend of L was only significant for forest, while the negative trend with soil depth (z) was only significant for grassland sites. The contact time of the water film with the soil matrix (T_D-T_w) showed no clear pattern and was not significant for any landscape unit.

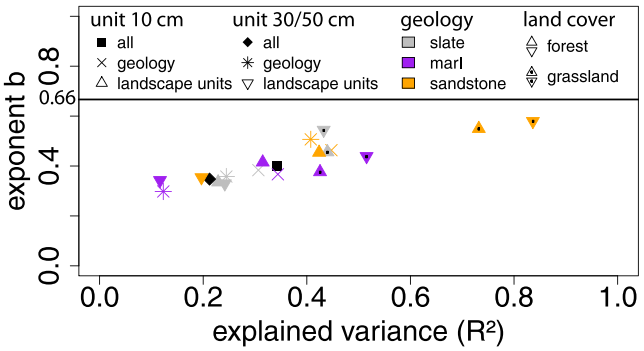

Figure 5. Relationship of explained variance (R^2) and the film flow exponent b for grouping the sites of different units (all, geology, landscape units) and the two depth.

4. Discussion

In this study, a gravity-driven film flow approach was tested in a diversity of geologies and land covers to describe preferential flow (PF). However, not all infiltration events met the defined criteria (Section 2.3) for fitting a WCW and further explorations on the reasons behind are necessary. Possible explanations are high water abstraction of the matrix, turbulent flow or a stronger contribution of capillary flow. However, also many events that were excluded due to one of the aforementioned reasons often showed a fast increase in water content (wetting front shock) as postulated by the film flow. However, for some other events (fitted and non-fitted events) the wetting front sometimes did not arriving as a wetting front shock but was rather gradually increasing, although still fast and with the typical shape of a WCW. Reasons could be the assumption of a homogenous rainfall pulse that is not given when using real world

Table 5
Comparison of Model Quality and Error Dependent on the Predicted Parameter

	F (individual fitted exponent)	$F + L$ (exponent = 2/3)
S_{opt} [−]	0.28	0.26
Median KGE [−]	0.66	0.22
Median error $\Delta\theta$ [−]	−0.0004	0.0052
0.25 quantile error $\Delta\theta$ [−]	−0.0019	0.0018
0.75 quantile error $\Delta\theta$ [−]	0.0009	0.0079
Max error $\Delta\theta$ [−]	0.0435	0.0470

data or a potential sensor lag as found for time domain reflectometry signals by Germann (2017).

The derived parameters of film flow are in the same range as parameters observed by Germann and Prasuhn (2018) or Germann and Karlen (2016) in a lysimeters or during sprinkling studies, respectively. Notably, Hincapié and Germann (2009b) found wetting front velocities and film thicknesses one magnitude higher than that demonstrated by our study. One explanation may be the higher sprinkling intensities (20 and 100 mm h^{-1}) under controlled conditions compared to the intensities of most infiltration events observed in our analysis. Furthermore, the higher v values found by Hincapié and Germann (2009b) demonstrate the variability of possible flow processes in different soils. Higher wetting front velocities in forests and in soils containing higher clay content (slate, marl) than in sandstone were observed. Such disparity in wetting front velocities can be attributed to higher macroporosity in these soils due to soil structure development (Alaoui et al., 2011; Stewart et al., 2016). Additionally, the marl geology likely reveals a higher velocity due to the high earthworm abundance and the higher number of biopores (Reck et al., 2018). Due to PF in secondary pores, a higher clay content does not necessarily correspond to slower flow velocity (Baram et al., 2012) as predicted by capillary driven matrix flow calculations.

The observed increase in wetting front velocity with depth for all soils is surprising since a decrease of hydraulic conductivity with depth has been frequently observed (Ameli et al., 2016; Libohova et al., 2018; Weiler & McDonnell, 2007). Uncertainty in the determination of the input pulse strongly influences wetting front velocity and the influence would be larger for sensors closer to the surface since longer flow distance compensates for the error. Subsequently, the question arises whether the beginning and the end of the measured rainfall pulse really does reflect the beginning and the end of infiltration and further if variable T_b and T_s in the optimization procedure is able to capture this phenomenon (see also Supporting Information Table S2: GLO-P). Some studies demonstrated that litter interception (Gerrits et al., 2007) or surface repellency due to hydrophobicity (Doerr et al., 2000) are processes that can prevent or decelerate infiltration. Other authors found an increase of the wetting front velocity with depth due to texture contrasting soils (Hardie et al., 2013), but since the increase was observed in all of our landscape units it is probably more related to the uncertainty of defining the beginning of infiltration. If the input estimation was correct, maybe saturation at the surface or in depressions is required to initiate film flow, especially at low rainfall intensities, as has been already observed for macropore flow initiation (Weiler & Naef, 2003b). Or and Tuller (2000) modeled film flow on rough surfaces and from their calculations it was shown that film flow is a dominating process at tension <50 hPa. A precise knowledge of the rain pulse beginning, end and duration is essential for an adequate determination of the wetting front velocity. Using the input from the fit of the upper sensor location could be a potential alternative that furthermore provides differentiated results with depth (see Supporting Information Tables S2 and S3: GLO-SM). We think that a water content sensor close to the soil surface might be more appropriate to determine the beginning of the input flux instead of measuring precipitation.

The function between precipitation intensity (q_s) and wetting front velocity (v) was able to explain a large proportion of the v-variance, depending on the landscape unit. The exponents of the power law relationships were always lower than 2/3, but better fits have resulted in exponents closer to 2/3. The most homogeneous groups such as sandstone grassland produces good fits (Figure 5). Since especially forest soils showed the lowest R^2 this is probably caused by uncertainties to determine the input flux. The observed throughfall is not necessarily the same rainfall input that reaches the instrumented soil profiles due to heterogeneous throughfall patterns (Keim et al., 2005). Also stemflow can change the input pulse at certain locations and does not reflect the throughfall measurements of our tipping buckets (Johnson & Lehmann, 2006; Schwärzel et al., 2012).

An exponent of 2/3 would indicate that the specific contact area (L) contributing to flow is independent from the input rate ($dL/dq_s = 0$). This would enable for the full applicability of film flow with kinematic wave theory (Germann & Karlen, 2016). If the kinematic wave theory could be applied, it would help to

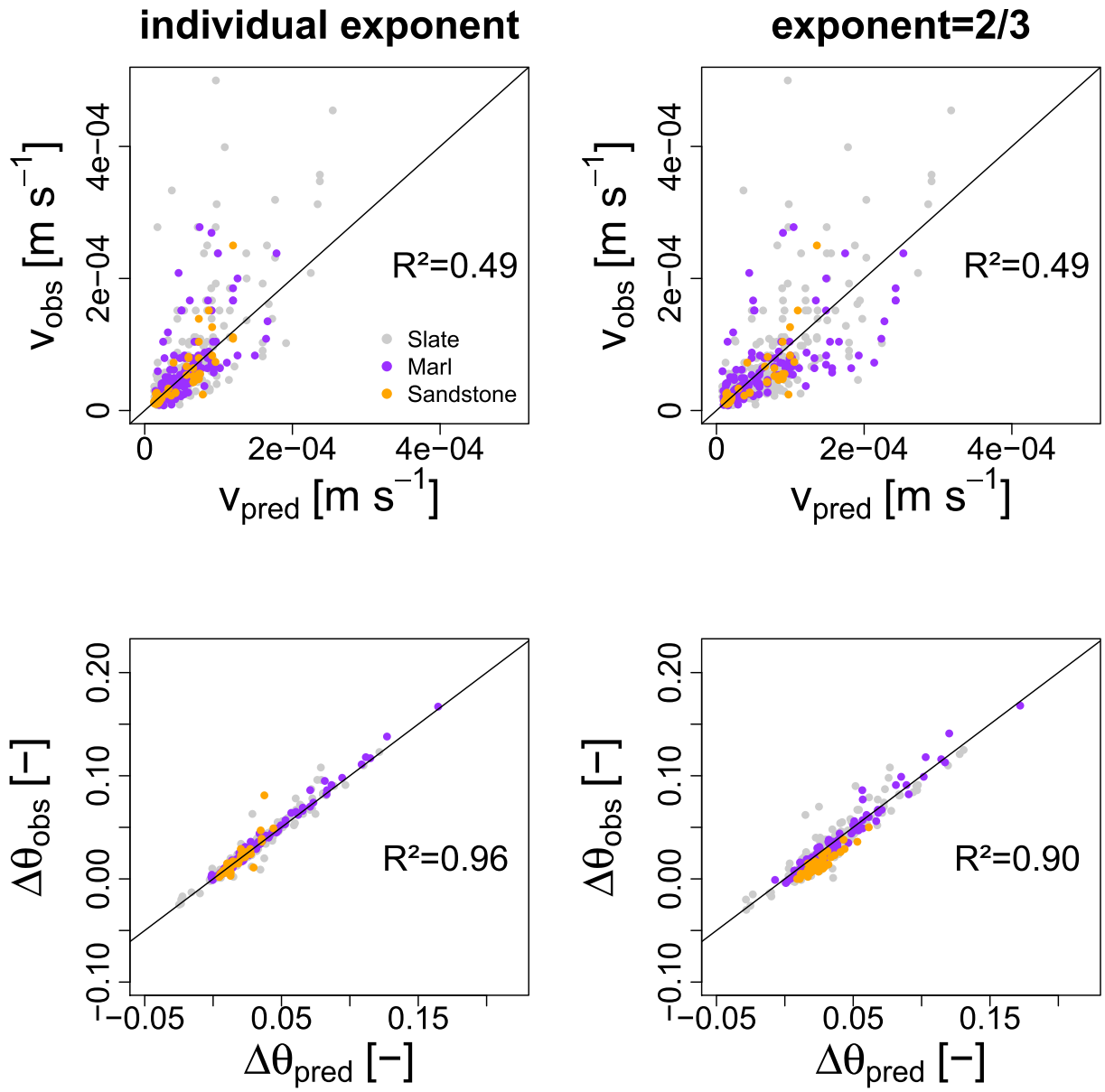

Figure 6. Comparison of model results by using the predicted (pred) parameters F or $F + L$ against the optimized or measured (obs) WCWs from the grassland sites. Colors indicate the different geologies. Left plots show the velocity prediction and water content change ($\Delta\theta$) for the case the parameter F is predicted from the observed relationship with rain intensity. The right diagrams evaluate the $F + L$ prediction by assuming an exponent of 2/3 in the power law relationship and calculating L from the fit. The lines represent the 1:1 relationships. WCW, water content wave.

model longer rain events with varying intensities by superimposition of multiple waves from single homogenous rain pulses (Germann, 2014; Germann & Karlen, 2016). Also rivulets routing down waves with different properties (F and L) could then be applied (Germann et al., 2007). Furthermore $dL/dq_s = 0$ would also allow to determine an average L from the v-q_s relationship, as we have tested for our landscape units. Germann et al. (2012) found a good agreement of site-specific L with the root density, which we have not measured and therefore could not test.

The observed deviation of the exponent from 2/3 in our study does not implicitly indicate $dL/dq_s \neq 0$. The first reason that the exponent is not 2/3 could be, as already discussed above, an incorrect determination of either v or q_s due to the uncertainty of approximating the duration of the rain pulse, including the assumption of a homogenous input pulse. An incorrect determination of the input flux in forests, as discussed above, is probably the most suitable explanation of the larger heterogeneity in the forest. Errors in v also

Table 6
Parameters of the Power Law Function to Predict the Wetting Front Velocity (Equation 15) Incorporating Input Flux (Rainfall Intensity) and Storage State (Initial Volumetric Water Content)

		10 cm				30/50 cm			
		a	b	n	R^2	a	b	n	R^2
Forest	Slate	0.0021	0.32	−0.29	0.25	0.0025	0.29	−0.55	0.27
	Marl	0.0264	0.43	0.22	0.32	0.0653	0.39	0.61	0.14
	Sandstone	0.0050	0.41	−0.54	0.47	0.0221	0.38	0.27	0.22
Grassland	Slate	0.0245	0.46	0.20	0.45	**0.1352**	**0.55**	**0.16**	0.43
	Marl	0.0060	0.37	−0.13	0.43	**0.1641**	**0.50**	**0.77**	0.55
	Sandstone	0.0137	0.51	−0.57	0.76	**0.1194**	**0.58**	**0.06**	0.84

Note. The values in bold are used for the comparison with HYDRUS 1D.

arise from the limited accuracy to determine v from soil moisture data with only 5-min resolution (see Supporting Information Figure S1). Furthermore, the observed water abstraction by the matrix (θ_{abs}) can lead to a different film thickness (F) than actually predicted for a specific q_s. The second reason for a derivation of the exponent from 2/3 is the assumed homogeneity among the single profiles of our landscape units. Since not every instrumented soil profile covers the complete range of q_s values, the regression may not accurately predict the v-q_s relationship. Additionally, the temporal change (e.g., seasonality) of the velocity-modulation coefficient (a) may not be similar for every profile of our landscape units and hence the regression can also be biased. The dL/dq_s properties should certainly be examined in more detail for different natural soils in the future, but the v-q_s relationships found for the grasslands in this study hint toward the case that film flow shows a relatively constant L with rain intensity (b close to 2/3) and the observed deviation of the exponent b from 2/3 leads to relatively small errors (Figure 6). A reasonable fit of the v-q_s function could potentially be used to identify landscapes that are more homogenous and hence may be suitable as representative units for a set of film flow parameters.

We demonstrated that the predictions of F and L from rainfall intensity in the more homogenous grasslands was possible for large scale landscape units with only introducing little error in both, the predicted wetting front velocity and the water content change. We are aware that the evaluation of the predicted film flow parameters was performed with the same data set as the fit. Nevertheless, predictions showed reasonable agreement with the measured or fitted data. Using an independent data set for validation could be an interesting study in the future.

Adding the influence of the water content to the physical relationships of the film flow model did only slightly improve the fit of the v-q_s function and the exponent b stayed relatively constant. We conclude that the initial water content has only a minor influence on gravity-driven film flow during infiltration. Hincapié and Germann (2009a) found a significant relationship of v-θ_{ini} in a few depth for one soil using a univariate linear regression. However, our analysis included different soil types, land covers, and seasonal varying events. The unclear relationship between v and θ_{ini} (either positive or negative dependent on the landscape unit) can probably be associated with surface effects such as hydrophobicity or to the water abstraction by the soil matrix. The stronger influence of the input pulse and only small differences between the soil types as described by the film flow model supports the idea of macropore flow without capillary forcing, which is more affected by factors creating a connected macropore network (e.g., vegetation or soil fauna) (e.g., Beven & Germann, 1982) than only soil particle size distribution or retention characteristics. In contrast, capillary flow revealed the expected dominant control of θ_{ini} and therefore also on the soil type, which is the major soil property influencing the capillary forcing. Experimental evidence that the infiltration velocity is not increasing with θ_{ini} was found, for example, by Blume et al. (2009), Hardie et al. (2013) or Demand et al. (2019). Although comparing the absolute values of v was not the aim of this comparison, the differences between the HYDRUS 1D (parametrized by a pedotransfer-function; capillary matrix flow only) and the film flow results (functions based on measured data) indicate that soil matrix flow alone cannot describe infiltration into these soils without accounting for PF.

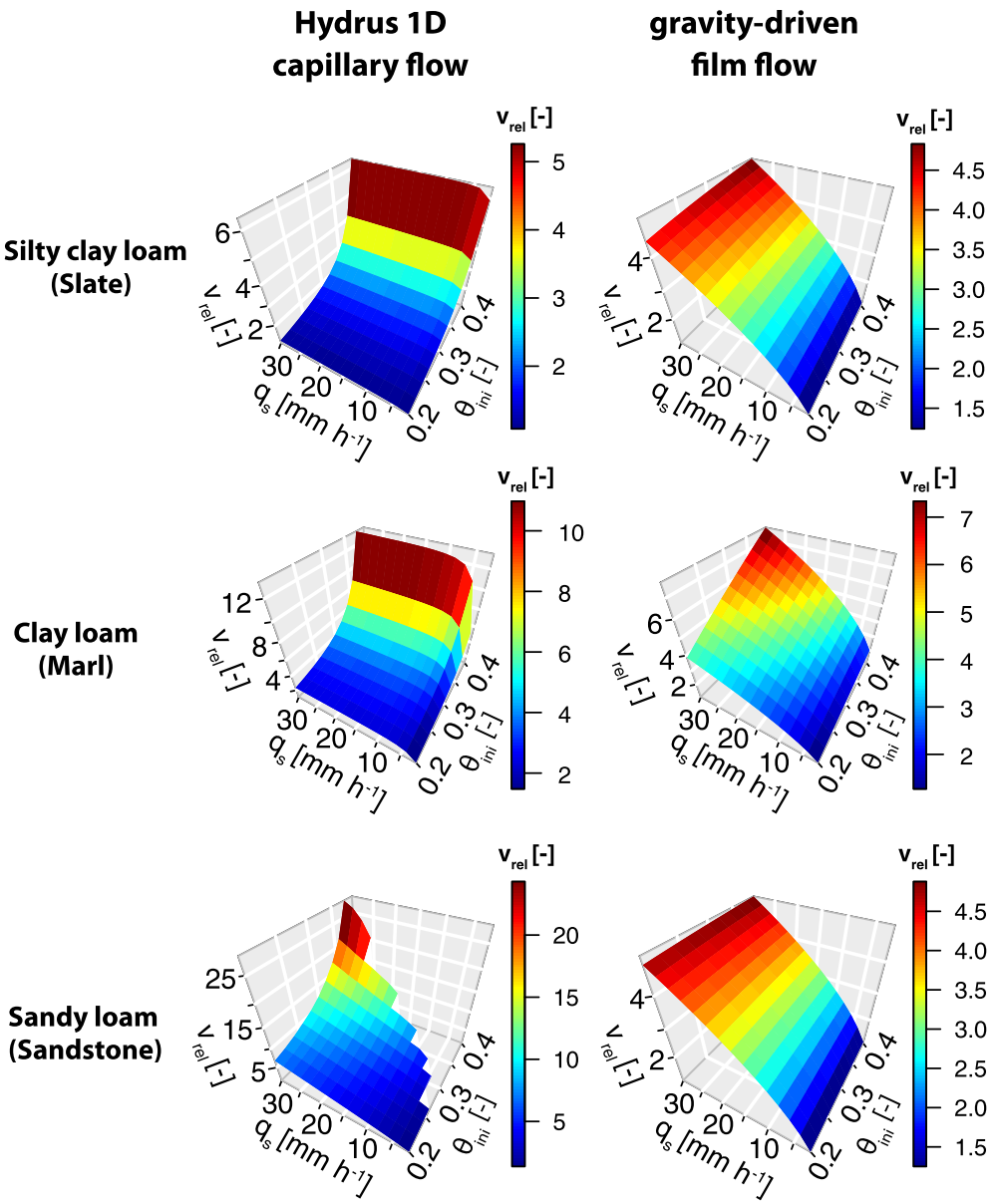

Figure 7. Comparison of relative increase in modeled wetting front velocities (v_{rel}) with rainfall pulse intensity (q_s) and initial water content (θ_{ini}) for the film flow and capillary flow (HYDRUS 1D) approach. Comparison was done for the three geologies of the grassland sites at 30 cm depth.

In contrast to the wetting front velocity, the water abstraction of the soil matrix (θ_{abs}) was more influenced by the geology than the land cover. With our multiple regression analysis θ_{abs} could not well predicted for the slate soils of both land covers. For the other landscape units, the analysis worked reasonably well, with plausible predictions of the regression. The multiple linear regression yielded higher water abstraction with a higher rainfall amount (water volume) and with more conducting interfaces (L). In contrast, we found less abstraction in deeper zones and less abstraction with higher initial water content due to the lower matric potential. Why the contact time of the water film with the soil matrix (T_D-T_w) can either result in a positive or negative trend is unclear yet. However, the relationships are not significant for any landscape unit. The possible processes behind the observed relationships needs more attention. For the soils on the slate geology the higher stone content was probably the reason for the lower quality of the fits. In general, the topic of water abstraction by the soil matrix during film flow was not given much attention in the past. Our approach was one of the first quite simple attempts using the parameters of the film flow to predict soil water storage

Table 7
Regression Coefficients of the Water Abstraction by the Soil Matrix (θ_{abs}) During Film Flow (17) for the Six Landscape Units (all Depth). α_1–α_5 are the Regression Coefficients and β is the intercept

		α_1 (θ_{ini} [−]) [$\times 10^{-2}$]	α_2 (P_{sum} [mm]) [$\times 10^{-4}$]	α_3 (L [m^2 m^{-3}]) [$\times 10^{-7}$]	α_4 (z [m]) [$\times 10^{-3}$]	α_5 (T_D-T_w [s]) [$\times 10^{-7}$]	β	R^2
Forest	Slate	−1.86	**3.17**	**14.36**	−0.62	2.94	**0.012**	0.26
	Marl	−3.36	**24.51**	**9.34**	14.36	−6.04	0.016	0.43
	Sandstone	**−15.28**	**6.87**	**9.07**	−9.07	3.09	**0.048**	0.49
Grassland	Slate	**−3.52**	**11.55**	−4.25	**−63.30**	5.20	**0.028**	0.13
	Marl	**−6.23**	**24.88**	3.51	**−86.03**	5.51	**0.034**	0.37
	Sandstone	**−9.19**	4.71	3.89	**−25.39**	−7.97	**0.045**	0.38

Note. Significant coefficients ($p < 0.01$) are marked with bold values.

change. More studies are needed in future to examine this process in more detail including feedback of the abstracted water to the water film in the macropore. Small scale soil properties such as texture, rock fraction or soil organic matter may be dominant factors influencing the soil water storage (Naseri et al., 2019; Saxton & Rawls, 2006). Hincapié and Germann (2009a) also tested the effect of θ_{ini} and q_s on the change in water content and showed that θ_{ini} affected θ_{end}, but q_s did not. Germann and Karlen (2016) found no remarkable impact of θ_{ini} on θ_{end} in their experiments and the sink term approach invented by Germann & Beven (1985) also failed when applied with a film flow model (Germann, 2014).

Another challenge when predicting θ_{abs} could be the missing knowledge on the geometry of the PF—matrix interaction. This could be tested by assuming hypothetical geometries (e.g., cube, sphere, tube, etc.) of the soil aggregates or flow path and calculating the resulting structures (e.g., number of pores, size of aggregates) based on the determined L parameter. Larsbo et al. (2005) implemented such a relationship in the MACRO model with a rectangular-slab geometry of the aggregates, Weiler (2005) for cylindrical macropores and Steinbrich et al. (2016) for crack networks. θ_{abs} is an essential part for the applicability of the approach and needs further research. Including a better prediction of θ_{abs} in the film flow would furthermore extend the approach to a new kind of dual-porosity model.

Our study shows the potential to apply a gravity-driven film flow theory in the future at the catchment scale with a low parameter demand and an option to predict these parameters. Of course, many processes are in fact controlled by capillary matrix flow, such as water redistribution, soil evaporation, root water uptake or slow matrix drainage. However, as far as Richards equation is involved, the fast gravity driven flow is just a "fitting domain" including all uncertainty of the predicted hydraulic properties for the matrix domain. Since capillary driven matrix flow may be marginal compared to PF during infiltration, we propose to integrate all flux during infiltration into one gravity driven domain with a model of low parameter demand, such as film flow. After the cessation of the rain events the model would switch, for example, to a capillary driven model (Richards) for describing the capillary dominated processes. A potential termination criterion for film flow was presented in this study, based on the decline of the mobile water content. This type of model can be seen as a "dual-response model," with a gravity driven flow domain for storage filling and a Richards domain for drainage and root water uptake. Determining the parameters of the film flow model for other soil moisture sensor networks in different climates and ecosystems is, however, necessary to find and establish relationships or pedotransfer-functions to predict the parameters of film flow.

5. Conclusions

Film flow was fitted to ~1,700 infiltration events at 135 instrumented soil profiles in a complex (geology, land cover) large-scale soil moisture sensor network to describe PF. Faster flow was found in forest compared to grassland sites. Furthermore, in contrast to capillary flow, clayey soils showed higher wetting front velocities compared to sandy textures. We further confirmed the theoretical relationship between rain intensity and wetting front velocity, but a more precise determination of input fluxes and initiation processes of infiltration is essential, especially in forests. For grasslands in different geological settings these

relationships can be used to predict film flow parameters with a reasonable accuracy. A further exploration and proof of the wetting front velocity to rainfall intensity relationship can improve applicability of the model to longer events and facilitates parameter prediction. Including the initial soil water content into the film flow model did not substantially improve the estimated relationships. The comparison with a capillary flow model (HYDRUS 1D) showed the dominance of the rainfall input properties in the film flow approach in contrast to the dominance of the initial soil moisture in the capillary flow model. More detailed studies how soil and site properties (e.g., texture, organic carbon, macropore, and aggregate geometry) and their temporal variation (structure formation and hydrophobicity) affect the soil matrix water abstraction from macropores should be realized in the future. Expanding the set of reliable transfer functions of the gravity-driven film flow (v-q_s, θ_{abs}) could help to implement the approach into catchment scale models using some kind of pedo-vegetation-transfer models. Film flow could further be combined with capillary driven flow in a dual-response model having an infiltration/filling and drainage domain. Alternative approaches, such as the film flow model presented here, could be a solution of the impediment of using the Richards equations and can thereby be strongly beneficial for water and solute transport on the catchment scale.

Appendix A

Film Thickness (F)

Due to the v-q_s (Equation 10) and v-F (Equation 3) relationships, also a direct connection between q_s and F exists. The film thickness F is needed for calculating for example, the mobile water content (Equation 1)

Combining Equations 3 and 10 leads to:

$$F(q_s) = \left({q_s}^{2/3} \left(\frac{g}{3\eta} \right)^{-2/3} L^{-2/3} \right)^{1/2} \tag{A1}$$

When defining:

$$k = \left(\frac{g}{3\eta} \right)^{-2/3} L^{-2/3} \tag{A2}$$

we can write Equation A1 as:

$$F(q_s) = \sqrt{k\, {q_s}^{b_2}}\ \ b_2 = 2/3 \tag{A3}$$

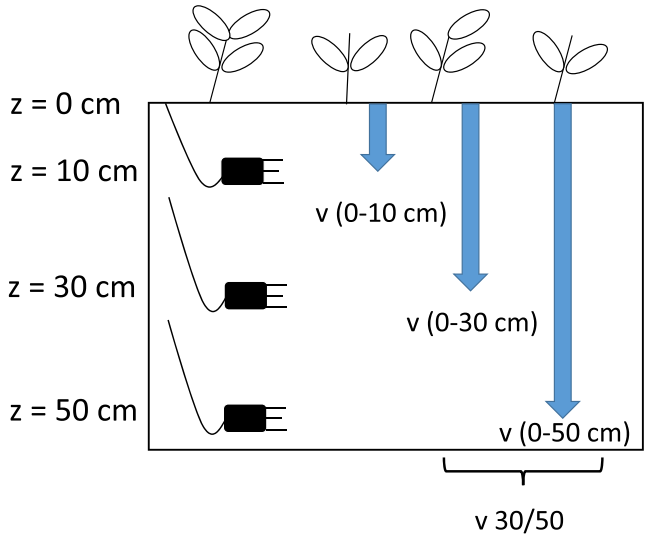

Figure A1. Schematic figure of the definition of measured wetting front **velocities.**

Figure A1 shows these relationships for the six landscape units. The slope of this log-log relationship (here denoted b_2) should also be 2/3 following the theory. However, the relationship of v to F involves the kinematic viscosity (Equation 3) that is not constant between the events due to temperature effects. Since the kinematic viscosity in the F-q_s (Figure A1) or v-q_s (Table 4) relationships is integrated into the parameter a or k respectively, these two power law relationships assume a constant viscosity and result in slightly differing slopes.

Average Specific Contact Area (L) Per Landscape Unit

To calculate the average L of a landscape unit based on the measured v-q_s relationship with a theoretical exponent $b = 2/3$ (Equation 11), the median kinematic viscosity of all events of each landscape unit and the two defined depths (10 or 30/50 cm) was used. The range of these average L values was between 3,711 and 13,149 $m^2\ m^{-3}$ for the different landscape units at 10 cm and 1,026–7,029 $m^2\ m^{-3}$ at 30/50 cm depth (Table A1).

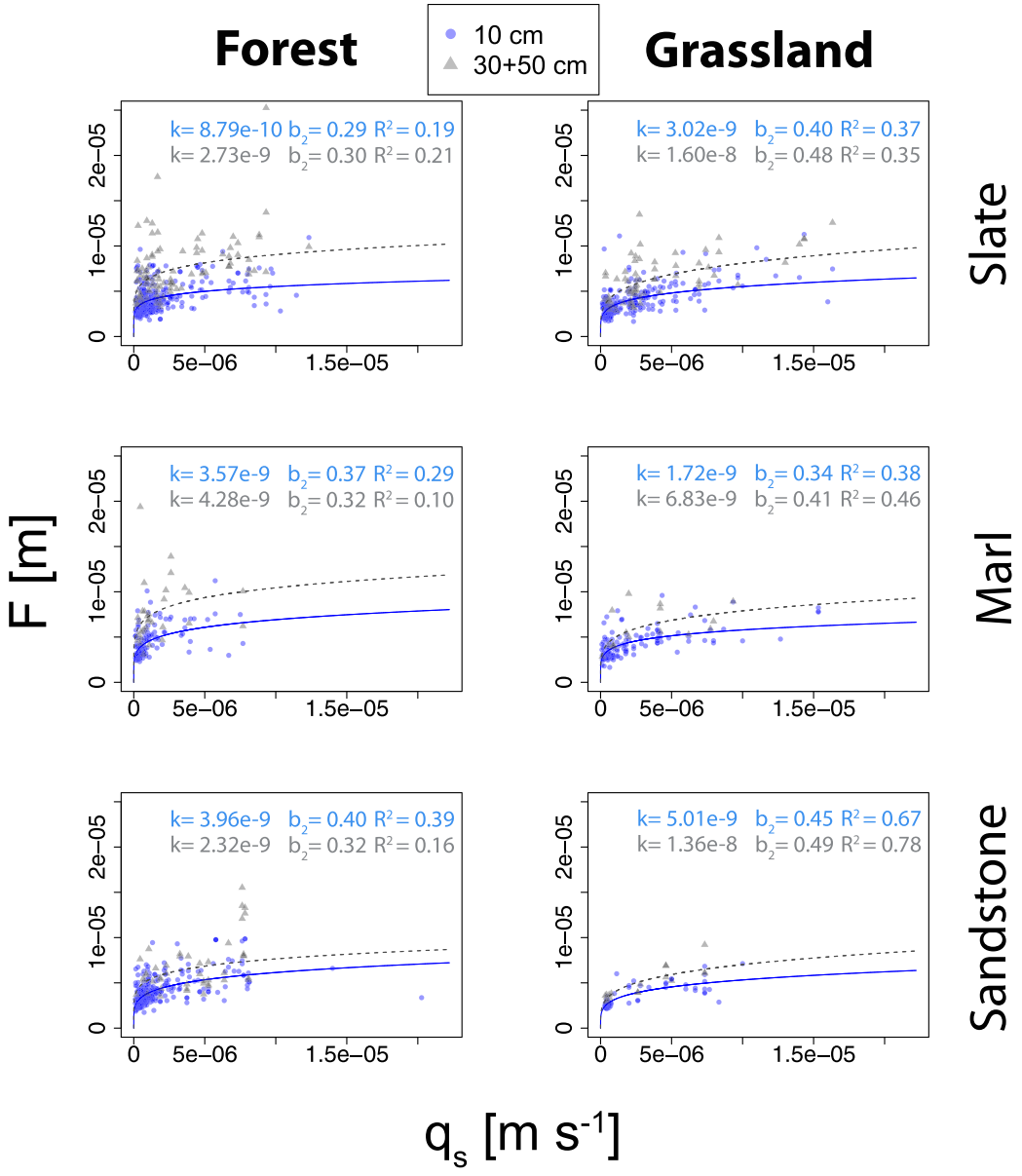

Figure A2. Relationships of the rainfall intensity (q_s) and the film thickness (F) as presented in Equation A3.

Marl forest showed the lowest L and sandstone grassland the highest at both depth classes. The general trend is similar to the wetting front velocity, but reversed. The forests exhibit lower L than the grasslands of the same geology, 30/50 cm parameters are always lower than 10 cm for the same landscape unit and within a land cover L is increasing from marl to slate to sandstone.

Table A1
Average L Parameter for the Different Landscape Units and Two Depth Classes Calculated by Using the Film Flow Relationship With a Fixed Exponent of 2/3

		Forest			Grassland		
	Depth [cm]	Slate	Marl	Sandstone	Slate	Marl	Sandstone
L[m^2 m^{-3}]	10	6586	3711	7182	9985	6767	13149
	30/50	1966	1026	4302	4772	3867	7029

Data Availability Statement

The data used in this study are freely available on the "FreiDok plus" repository of the University of Freiburg: https://freidok.uni-freiburg.de/data/194286

Acknowledgments
This project was funded by the German Research Association (DFG): FOR 1598 - From Catchments as Organized Systems to Models based on Dynamic Functional Units–CAOS. Special thanks to Theresa Blume, Britta Kattenstroth, Tobias Vetter and many other helpers for the installation and maintenance of the field sites. We acknowledge the comments of John Nimmo, Ryan Stewart and one anonymous reviewer which greatly improved this study. Peter Germann unfortunately passed away before this study was published, but we have highly acknowledged the inspiring discussions we had with him, which provided us many new perspectives on viscous film flow.

References

Alaoui, A., Caduff, U., Gerke, H. H., & Weingartner, R. (2011). Preferential flow effects on infiltration and runoff in grassland and forest soils. *Vadose Zone Journal*, *10*(1), 367–377. https://doi.org/10.2136/vzj2010.0076

Ameli, A. A., McDonnell, J. J., & Bishop, K. (2016). The exponential decline in saturated hydraulic conductivity with depth: A novel method for exploring its effect on water flow paths and transit time distribution. *Hydrological Processes*, *30*(14), 2438–2450. https://doi.org/10.1002/hyp.10777

Armstrong, A. C., Matthews, A. M., Portwood, A. M., Leeds-Harrison, P. B., & Jarvis, N. J. (2000). CRACK-NP: A pesticide leaching model for cracking clay soils. *Agricultural Water Management*, *44*(1–3), 183–199. https://doi.org/10.1016/s0378-3774(99)00091-8

Arora, B., Mohanty, B. P., & McGuire, J. T. (2011). Inverse estimation of parameters for multidomain flow models in soil columns with different macropore densities. *Water Resources Research*, *47*(4). https://doi.org/10.1029/2010wr009451

Arora, B., Mohanty, B. P., & McGuire, J. T. (2012). Uncertainty in dual permeability model parameters for structured soils. *Water Resources Research*, *48*(1). https://doi.org/10.1029/2011wr010500

Baer, J. U., Kent, T. F., & Anderson, S. H. (2009). Image analysis and fractal geometry to characterize soil desiccation cracks. *Geoderma*, *154*(1–2), 153–163. https://doi.org/10.1016/j.geoderma.2009.10.008

Baram, S., Kurtzman, D., & Dahan, O. (2012). Water percolation through a clayey vadose zone. *Journal of Hydrology*, *424–425*(425), 165–171. https://doi.org/10.1016/j.jhydrol.2011.12.040

Beckers, J., & Alila, Y. (2004). A model of rapid preferential hillslope runoff contributions to peak flow generation in a temperate rain forest watershed. *Water Resources Research*, *40*(3), 1–19. https://doi.org/10.1029/2003wr002582

Beven, K., & Germann, P. (1981). Water flow in soil macropores II. A combined flow model. *Journal of Soil Science*, *32*(1), 15–29. https://doi.org/10.1111/j.1365-2389.1981.tb01682.x

Beven, K., & Germann, P. (1982). Macropores and water flow in soils. *Water Resources Research*, *18*(5), 1311–1325. https://doi.org/10.1029/wr018i005p01311

Beven, K., & Germann, P. (2013). Macropores and water flow in soils revisited. *Water Resources Research*, *49*(6), 3071–3092. https://doi.org/10.1002/wrcr.20156

Blume, T., Zehe, E., & Bronstert, A. (2009). Use of soil moisture dynamics and patterns at different spatio-temporal scales for the investigation of subsurface flow processes. *Hydrology and Earth System Sciences*, *13*, 1215–1233. https://doi.org/10.5194/hess-13-1215-2009

Campbell, G. S. (1974). A simple method for determining unsaturated conductivity from moisture retention data. *Soil Science*, *117*(6), 311–314. https://doi.org/10.1097/00010694-197406000-00001

Carsel, R. F., & Parrish, R. S. (1988). Developing joint probability distributions of soil water retention characteristics. *Water Resources Research*, *24*(5), 755–769. https://doi.org/10.1029/wr024i005p00755

DecagonDevices. (2016). 5TE Water contant, EC and temperature sensor, version: March 11, 2016 —11:55:57. Retrieved from http://manuals.decagon.com/Retired%20and%20Discontinued/Manuals/13509_5TE_Web.pdf

Demand, D., Blume, T., & Weiler, M. (2019). Spatio-temporal relevance and controls of preferential flow at the landscape scale. *Hydrology and Earth System Sciences*, *23*, 4869–4889. https://doi.org/10.5194/hess-23-4869-2019

Diamantopoulos, E., & Durner, W. (2012). Dynamic nonequilibrium of water flow in porous media: A review. *Vadose Zone Journal*, *11*(3). https://doi.org/10.2136/vzj2011.0197

DIN ISO 11277. (2002). *11277: Soil quality—Determination of particle size distribution in mineral soil material—Method by sieving and sedimentation* (ISO 11277:1998 + ISO 11277:1998 Corrigendum 1:2002).

Di Pietro, L., Ruy, S., & Capowiez, Y. (2003). Predicting preferential water flow in soils by traveling-dispersive waves. *Journal of Hydrology*, *278*(1–4), 64–75. https://doi.org/10.1016/s0022-1694(03)00124-0

Doerr, S. H., Shakesby, R. A., & Walsh, R. P. D. (2000). Soil water repellency: Its causes, characteristics and hydro-geomorphological significance. *Earth-Science Reviews*, *51*(1–4), 33–65. https://doi.org/10.1016/s0012-8252(00)00011-8

Durner, W. (1994). Hydraulic conductivity estimation for soils with heterogeneous pore structure. *Water Resources Research*, *30*(2), 211–223. https://doi.org/10.1029/93wr02676

Gerke, H. H., & Köhne, J. M. (2004). Dual-permeability modeling of preferential bromide leaching from a tile-drained glacial till agricultural field. *Journal of Hydrology*, *289*(1–4), 239–257. https://doi.org/10.1016/j.jhydrol.2003.11.019

Gerke, H. H., & van Genuchten, M. T. (1993). A dual-porosity model for simulating the preferential movement of water and solutes in structured porous media. *Water Resources Research*, *29*(2), 305–319. https://doi.org/10.1029/92wr02339

Germann, P. F. (1985). Kinematic wave approach to infiltration and drainage into and from soil macropores. *Transactions of the ASAE*, *28*(3), 745–749.

Germann, P. F. (2014). *Preferential flow: Stokes approach to infiltration and drainage* (Geographica Bernensia G88). Inst. of Geography, University of Bern.

Germann, P. F. (2017). Shape of time domain reflectometry signals during the passing of wetting fronts. *Vadose Zone Journal*, *16*(2). https://doi.org/10.2136/vzj2016.08.0070

Germann, P. F., & al Hagrey, S. A. (2008). Gravity-driven and viscosity-dominated infiltration into a full-scale sand model. *Vadose Zone Journal*, *7*(4), 1160–1169. https://doi.org/10.2136/vzj2007.0172

Germann, P. F., & Beven, K. (1985). Kinematic wave approximation to infiltration into soils with sorbing macropores. *Water Resources Research*, *21*(7), 990–996. https://doi.org/10.1029/wr021i007p00990

Germann, P. F., & DiPietro, L. (1996). When is porous-media flow preferential? A hydromechanical perspective. *Geoderma*, *74*(1–2), 1–21. https://doi.org/10.1016/s0016-7061(96)00059-6

Germann, P. F., & Di Pietro, L. (1999). Scales and dimensions of momentum dissipation during preferential flow in soils. *Water Resources Research*, *35*(5), 1443–1454. https://doi.org/10.1029/1998wr900112

Germann, P. F., Helbling, A., & Vadilonga, T. (2007). Rivulet approach to rates of preferential infiltration. *Vadose Zone Journal*, *6*(2), 207–220. https://doi.org/10.2136/vzj2006.0115

Germann, P. F., & Hensel, D. (2006). Poiseuille flow geometry inferred from velocities of wetting fronts in soils. *Vadose Zone Journal*, *5*(3), 867–876. https://doi.org/10.2136/vzj2005.0080

Germann, P. F., & Karlen, M. (2016). Viscous-flow approach to in situ infiltration and in vitro saturated hydraulic conductivity determination. *Vadose Zone Journal*, *15*(2). https://doi.org/10.2136/vzj2015.05.0065

Germann, P. F., Lange, B., & Lüscher, P. (2012). Preferential flow dynamics and plant rooting systems. In H. Lin (Ed.), *Hydropedology* (pp. 121–141). Academic Press. https://doi.org/10.1016/B978-0-12-386941-8.00004-6

Germann, P. F., & Prasuhn, V. (2018). Viscous flow approach to rapid infiltration and drainage in a weighing lysimeter. *Vadose Zone Journal*, *17*(1). https://doi.org/10.2136/vzj2017.01.0020

Gerrits, A. M. J., Savenije, H. H. G., Hoffmann, L., & Pfister, L. (2007). New technique to measure forest floor interception—An application in a beech forest in Luxembourg. *Hydrology and Earth System Sciences*, *11*(2), 695–701. https://doi.org/10.5194/hess-11-695-2007

Hardie, M., Lisson, S., Doyle, R., & Cotching, W. (2013). Determining the frequency, depth and velocity of preferential flow by high frequency soil moisture monitoring. *Journal of Contaminant Hydrology*, *144*(1), 66–77. https://doi.org/10.1016/j.jconhyd.2012.10.008

Haws, N. W., Rao, P. S. C., Simunek, J., & Poyer, I. C. (2005). Single-porosity and dual-porosity modeling of water flow and solute transport in subsurface-drained fields using effective field-scale parameters. *Journal of Hydrology*, *313*(3–4), 257–273. https://doi.org/10.1016/j.jhydrol.2005.03.035

Hincapié, I., & Germann, P. F. (2009a). Impact of initial and boundary conditions on preferential flow. *Journal of Contaminant Hydrology*, *104*(1–4), 67–73. https://doi.org/10.1016/j.jconhyd.2008.10.001

Hincapié, I. A., & Germann, P. F. (2009b). Abstraction from infiltrating water content waves during weak viscous flows. *Vadose Zone Journal*, *8*(4), 996–1003. https://doi.org/10.2136/vzj2009.0012

Iden, S. C., & Durner, W. (2014). Comment on "simple consistent models for water retention and hydraulic conductivity in the complete moisture range" by A. Peters. *Water Resources Research*, *50*(9), 7530–7534. https://doi.org/10.1002/2014wr015937

Ippisch, O., Vogel, H.-J., & Bastian, P. (2006). Validity limits for the van Genuchten-Mualem model and implications for parameter estimation and numerical simulation. *Advances in Water Resources*, *29*(12), 1780–1789. https://doi.org/10.1016/j.advwatres.2005.12.011

IUSS Working Group WRB. (2006). *World reference base for soil resources 2006 (World Soil Resources Reports No. 103)*. FAO.

Jackisch, C., & Zehe, E. (2018). Ecohydrological particle model based on representative domains. *Hydrology and Earth System Sciences*, *22*(7), 3639–3662. https://doi.org/10.5194/hess-22-3639-2018

Jarvis, N. J. (2007). A review of non-equilibrium water flow and solute transport in soil macropores: Principles, controlling factors and consequences for water quality. *European Journal of Soil Science*, *58*(3), 523–546. https://doi.org/10.1111/j.1365-2389.2007.00915.x

Jarvis, N. J., Jansson, P.-E., Dik, P. E., & Messing, I. (1991). Modeling water and solute transport in macroporous soil. I. Model description and sensitivity analysis. *Soil Science*, *42*(1), 59–70. https://doi.org/10.1111/j.1365-2389.1991.tb00091.x

Jarvis, N. J., Koestel, J., & Larsbo, M. (2017). Reply to 'Comment on "Understanding preferential flow in the Vadose zone: Recent advances and future prospects" by N. Jarvis et al. *Vadose Zone Journal*, *16*(5). https://doi.org/10.2136/vzj2017.01.0034r

Johnson, M. S., & Lehmann, J. (2006). Double-funneling of trees: Stemflow and root-induced preferential flow. *Écoscience*, *13*(3), 324–333. https://doi.org/10.2980/i1195-6860-13-3-324.1

Keim, R. F., Skaugset, A. E., & Weiler, M. (2005). Temporal persistence of spatial patterns in throughfall. *Journal of Hydrology*, *314*(1–4), 263–274. https://doi.org/10.1016/j.jhydrol.2005.03.021

Klaus, J., & Zehe, E. (2010). Modeling rapid flow response of a tile-drained field site using a 2D physically based model: assessment of 'equifinal' model setups. *Hydrological Processes*, *24*(12), 1595–1609. https://doi.org/10.1002/hyp.7687

Kling, H., Fuchs, M., & Paulin, M. (2012). Runoff conditions in the upper Danube basin under an ensemble of climate change scenarios. *Journal of Hydrology*, *424–425*(425), 264–277. https://doi.org/10.1016/j.jhydrol.2012.01.011

Kodesova, R., Šimůnek, J., Nikodem, A., & Jirku, V. (2010). Estimation of the dual-permeability model parameters using tension Disk Infiltrometer and Guelph Permeameter. *Vadose Zone Journal*, *9*(2), 213–225. https://doi.org/10.2136/Vzj2009.0069

Köhne, J. M., Köhne, S., & Gerke, H. H. (2002). Estimating the hydraulic functions of dual-permeability models from bulk soil data. *Water Resources Research*, *38*(7), 261–2611. https://doi.org/10.1029/2001WR000492

Köhne, J. M., Köhne, S., & Šimůnek, J. (2009). A review of model applications for structured soils: a) Water flow and tracer transport. *Journal of Contaminant Hydrology*, *104*(1–4), 4–35. https://doi.org/10.1016/j.jconhyd.2008.10.002

Larsbo, M., Roulier, S., Stenemo, F., Kasteel, R., & Jarvis, N. (2005). An Improved dual-permeability model of water flow and solute transport in the Vadose Zone. *Vadose Zone Journal*, *4*(2), 398–406. https://doi.org/10.2136/vzj2004.0137

Libohova, Z., Schoeneberger, P., Bowling, L. C., Owens, P. R., Wysocki, D., Wills, S., et al. (2018). Soil systems for upscaling saturated hydraulic conductivity for hydrological modeling in the critical zone. *Vadose Zone Journal*, *17*. https://doi.org/10.2136/vzj2017.03.0051

Logsdon, S. D. (2002). Determination of preferential flow model parameters. *Soil Science Society of America Journal*, *66*(4), 1095–1103. https://doi.org/10.2136/sssaj2002.1095

Merz, B., & Bárdossy, A. (1998). Effects of spatial variability on the rainfall runoff process in a small loess catchment. *Journal of Hydrology*, *212–213*(1–4), 304–317. https://doi.org/10.1016/s0022-1694(98)00213-3

Mullen, K., Ardia, D., Gil, D., Windover, D., & Cline, J. (2011). DEoptim : An R package for global optimization by differential evolution. *Journal of Statistical Software*, *40*(6), 1–26. https://doi.org/10.18637/jss.v040.i06

Naseri, M., Iden, S. C., Richter, N., & Durner, W. (2019). Influence of stone content on soil hydraulic properties: Experimental investigation and test of existing model concepts. *Vadose Zone J.*, *18*(1), 1–10. https://doi.org/10.2136/vzj2018.08.0163

Niehoff, D., Fritsch, U., & Bronstert, A. (2002). Land-use impacts on storm-runoff generation: Scenarios of land-use change and simulation of hydrological response in a meso-scale catchment in SW-Germany. *Journal of Hydrology*, *267*(1–2), 80–93. https://doi.org/10.1016/s0022-1694(02)00142-7

Nimmo, J. R. (2007). Simple predictions of maximum transport rate in unsaturated soil and rock. *Water Resources Research*, *43*(5), 139–141. https://doi.org/10.1029/2006wr005372

Nimmo, J. R. (2010). Theory for source-responsive and free-surface film modeling of unsaturated flow. *Vadose Zone Journal*, *9*(2), 295–306. https://doi.org/10.2136/vzj2009.0085

Nimmo, J. R. (2012). Preferential flow occurs in unsaturated conditions. *Hydrological Processes*, *26*(5), 786–789. https://doi.org/10.1002/hyp.8380

Or, D., & Tuller, M. (2000). Flow in unsaturated fractured porous media: Hydraulic conductivity of rough surfaces. *Water Resources Research*, *36*(5), 1165–1177. https://doi.org/10.1029/2000wr900020

Reck, A., Jackisch, C., Hohenbrink, T. L., Zangerlé, A., & Schaik, L. V. (2018). Impact of temporal macropore dynamics on infiltration: Field Experiments and model simulations. *Vadose Zone Journal*, *17*(1). https://doi.org/10.2136/vzj2017.08.0147

Richards, L. A. (1931). Capillary conduction of liquids through porous mediums. *Physics*, *1*, 318–333. https://doi.org/10.1063/1.1745010

Saxton, K. E., & Rawls, W. J. (2006). Soil water characteristic estimates by texture and organic matter for hydrologic solutions. *Soil Science Society of America Journal*, *70*(5), 1569. https://doi.org/10.2136/sssaj2005.0117

Schaap, M. G., Leij, F. J., & van Genuchten, M. T. (2001). Rosetta: A computer program for estimating soil hydraulic parameters with hierarchical pedotransfer functions. *Journal of Hydrology*, *251*, 163–176. https://doi.org/10.1016/s0022-1694(01)00466-8

Schwärzel, K., Ebermann, S., & Schalling, N. (2012). Evidence of double-funneling effect of beech trees by visualization of flow pathways using dye tracer. *Journal of Hydrology*, *470–471*(471), 184–192. https://doi.org/10.1016/j.jhydrol.2012.08.048

Shipitalo, M. J., Dick, W. A., & Edwards, W. M. (2000). Conservation tillage and macropore factors that affect water movement and the fate of chemicals. *Soil and Tillage Research*, *53*, 167–183. https://doi.org/10.1016/s0167-1987(99)00104-x

Šimůnek, J., Šejna, M., Saito, H., Sakai, M., & van Genuchten, M. T. (2013). *The HYDRUS-1D Software Package for Simulating the Movement of Water, Heat, and Multiple Solutes in Variably Saturated Media, Version 4.17, HYDRUS Software Series 3*. Department of Environmental Sciences, University of California Riverside.

Sprenger, M., Tetzlaff, D., Buttle, J., Laudon, H., Leistert, H., Mitchell, C. P. J., et al. (2018). Measuring and modeling stable isotopes of mobile and bulk soil water. *Vadose Zone Journal*, *17*(1), 170149. https://doi.org/10.2136/vzj2017.08.0149

Steinbrich, A., Leistert, H., & Weiler, M. (2016). Model-based quantification of runoff generation processes at high spatial and temporal resolution. *Environmental Earth Sciences*, *75*(21), 1–16. https://doi.org/10.1007/s12665-016-6234-9

Stewart, R. D., Najm, M. R. A., Rupp, D. E., & Selker, J. S. (2016). Modeling multi domain hydraulic properties of shrink-swell soils. *Water Resources Research*, *52*, 5727–5754. https://doi.org/10.1002/2016wr019336

Storn, R., & Price, K. (1997). Differential evolution—A simple and efficient heuristic for global optimization over continuous spaces. *Journal of Global Optimization*, *11*(4), 341–359. https://doi.org/10.1023/a:1008202821328

Tokunaga, T. K., & Wan, J. (1997). Water film flow along fracture surfaces of porous rock. *Water Resources Research*, *33*(6), 1287–1295. https://doi.org/10.1029/97wr00473

Topp, G. C., Davis, J. L., & Annan, A. P. (1980). Electromagnetic determination of soil water content: Measurements in coaxial transmission lines. *Water Resources Research*, *16*(3), 574–582. https://doi.org/10.1029/wr016i003p00574

van Genuchten, M. T. (1980). A closed-form equation for predicting the hydraulic conductivity of unsaturated soils. *Soil Science Society of America Journal*, *44*(5), 892–898. https://doi.org/10.2136/sssaj1980.03615995004400050002x

van Schaik, N. L. M. B., Hendriks, R. F. A., & van Dam, J. C. (2010). Parameterization of macropore flow using dye-tracer infiltration patterns in the SWAP model. *Vadose Zone Journal*, *9*(1), 95–106. https://doi.org/10.2136/vzj2009.0031

Vogel, H.-J., & Ippisch, O. (2008). Estimation of a critical spatial discretization limit for solving Richards' equation at large scales. *Vadose Zone Journal*, *7*(1), 112–114. https://doi.org/10.2136/vzj2006.0182

Vogel, H. J., & Roth, K. (1998). A new approach for determining effective soil hydraulic functions. *European Journal of Soil Science*, *49*(4), 547–556. https://doi.org/10.1046/j.1365-2389.1998.4940547.x

Weast, R. C. (1989). *CRC handbook of chemistry and physics* (69th ed.). CRC Press Inc.

Weiler, M. (2005). An infiltration model based on flow variability in macropores: Development, sensitivity analysis and applications. *Journal of Hydrology*, *310*(1–4), 294–315. https://doi.org/10.1016/j.jhydrol.2005.01.010

Weiler, M., & McDonnell, J. J. (2007). Conceptualizing lateral preferential flow and flow networks and simulating the effects on gauged and ungauged hillslopes. *Water Resources Research*, *43*(3), 1–13. https://doi.org/10.1029/2006wr004867

Weiler, M., & Naef, F. (2003). Simulating surface and subsurface initiation of macropore flow. *Journal of Hydrology*, *273*(1–4), 139–154. https://doi.org/10.1016/s0022-1694(02)00361-x